Technical Note	1975-6
Effects of Local Terrain and Obstacles Upon Near Horizon Gain of L-Band Beacon Antennas	A. Spiridon 17 July 1975

Prepared for the Federal Aviation Administration by

Lincoln Laboratory

MASSACHUSETTS INSTITUTE OF TECHNOLOGY

LEXINGTON, MASSACHUSETTS

1. Report No.	2. Government Accession No.	3. Recipient's Catalog No.
ESD-TR-75-224		

4. Title and Subtitle	5. Report Date
Effects of Local Terrain and Obstacles Upon Near Horizon Gain of L-Band Beacon Antennas	17 July 1975
	6. Performing Organization Code

7. Author(s)	8. Performing Organization Report No.
Spiridon, Alex	Technical Note 1975-6

9. Performing Organization Name and Address	10. Work Unit No. (TRAIS) 45364 034-241-012
Lincoln Laboratory, M.I.T. P.O. Box 73 Lexington, MA 02173	11. Contract or Grant No. IAG DOT-FA72WAI-261
	13. Type of Report and Period Covered

12. Sponsoring Agency Name and Address	
Department of Transportation Federal Aviation Administration Systems Research and Development Service Washington, DC 20591	Technical Note
	14. Sponsoring Agency Code

15. Supplementary Notes

16. Abstract

Models are given of the mechanisms that determine the effective gain of an L-band ground based antenna at near horizon elevation angles. Primary emphasis is given to the environment of typical Air Traffic Control Radar Beacon System (ATCRBS) sites.

17. Key Words	18. Distribution Statement
fade obstacle shadow vertical lobing	Document is available to the public through the National Technical Information Service, Springfield, Virginia 22151.

19. Security Classif. (of this report)	20. Security Classif. (of this page)	21. No. of Pages	
Unclassified	Unclassified	96	

TABLE OF CONTENTS

LIST OF ILLUSTRATIONS

LIST OF ILLUSTRATIONS (cont.)

LIST OF ILLUSTRATIONS (cont.)

LIST OF ILLUSTRATIONS (cont.)

LIST OF TABLES

I. INTRODUCTION

DABS, a ground based discrete address beacon system operating at L-band[*], provides surveillance and communications service for air traffic control. DABS ground based sensors will employ antennas with azimuth beam width of a few degrees and sector shaped elevation patterns to interrogate transponders in the aircraft. This report reviews issues related to DABS antenna fades. The term "fade," as it is used in this report, is defined as the amount by which the effective gain of an antenna deviates from its free space gain. Results are specialized to specific environments that are deemed important for the proper siting and performance of DABS sensors. Simplified models and criteria are given to describe the fade magnitudes to be expected in specific situations.

Only the DABS uplink fade mechanisms have been studied, since processes involved on the downlink are very similar. Attention has been focused on the field at long ranges from the sensor and within the first few degrees above the horizon. Two processes are studied in detail: the reflection of the field by surrounding terrain, and the modification of the direct field by objects within sight of the sensor. The direct and reflected field components make up the uplink field.

Several cases have been studied wherein the field is modified by a masking aperture or open aperture in the path of the field. The fade in the shadow of a building within sight of the sensor has been studied by representing the building as a shielding aperture. The buildings shown at A in Fig. 1 produce

_____

[*]DABS, vertically polarized (uplink), operates at 1030 mHz, and at 1090 mHz (downlink).

1
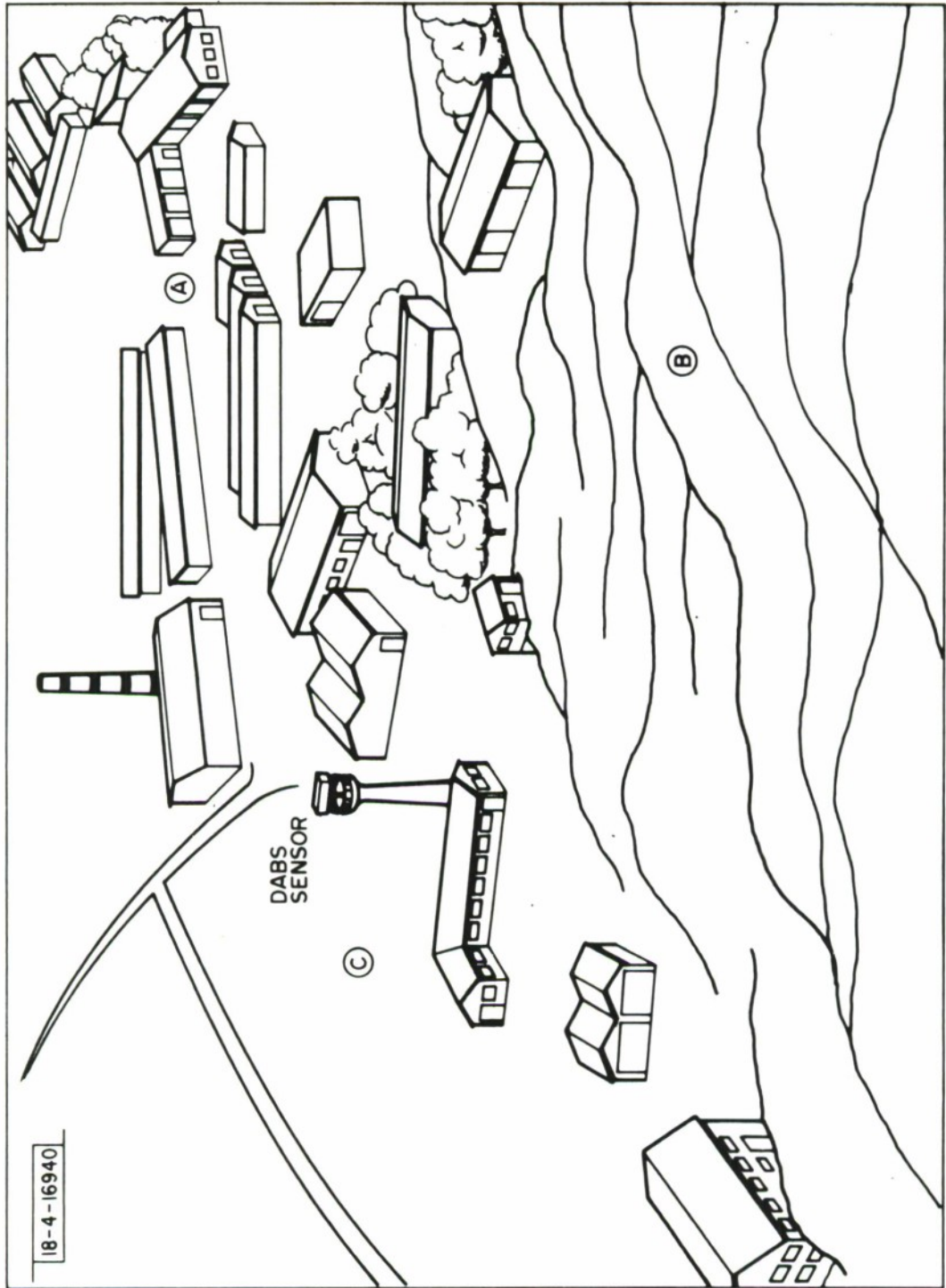
Fig. 1. DABS sensor and its environment.

such fades. A similar category of obstacles that shield the direct field are the hilltops represented by region B in Fig. 1. Each hilltop attenuates the field with the physical process corresponding to multiple edge diffraction (each edge being semi-infinite). The reflection of the field at an airport is modeled as an open aperture in the path of a field radiated by an image source. The limited flat terrain from the sensor to the built up area acts as a limited aperture. An example of this is shown in region C of Fig. 1.

Chapter II will review the field modification due to an aperture in the path of the field. This theory is used in Chapter III to examine the effect of a limited flat surface on reflected field. In Chapter IV the theory is used to evaluate the fade in the shadow of an obstacle. Multiple edge diffraction is discussed in Chapter V.

Two mechanisms involved in the reflection of the field in a hilly environment have been studied and their effects are reported. One such mechanism is shadowing by major hills resulting in a reduction of the reflected field. The other mechanism is scattering by local roughness, also resulting in a reduction of the reflected field. Region B in Fig. 1 illustrates such terrain. It is difficult to formulate a simple deterministic description of the above processes. Therefore, the problem has been statistically addressed. Optical theory has been used to describe the shadowing cast by hills. Such hilly terrain has been described as a Gaussian function. The result has been to show that the terrain that is visible to the sensor has been reduced, which in turn reduces the reflected field. A new model has been developed for shadowing, based on describing the terrain by isolated Poisson distributed hills. The advantage of the model is its

ability to take into account the nonstationary character of terrain roughness. The reflected field is also reduced, as a result of scattering, by the local roughness of the visible patches of terrain. Chapter VII discusses the effects of hill shadowing and local terrain roughness reflected in a hilly environment.

Chapter VI summarizes the literature on the attenuation of a field upon reflection from a flat surface.

A review of the effects of uplink propagation through the atmosphere (bending and reducing the speed of RF rays) is included. Such atmospheric propagation is a nonstationary process varying on a daily as well as on a seasonal basis to produce variations in field power. A beacon sensor uses the propagation round trip time to determine aircraft range. Consequently, it is critical to have an accurate value for the speed of light. The nonuniform index of refraction of the atmosphere, which decreases with altitude, bends the path of the RF uplink and reduces its speed. This results in an effective speed of light that is less than the speed of light. Appendix C summarizes the results of our study of atmospheric propagation as related to the ATCRBS or DABS link.

Figure 2 summarizes the issues discussed in this report and indicates chapters under which they are discussed.

4

Note: The first chapter of each block designates airport environment; the second chapter designates hilly environment.

Direct field

Sensor

Indirect field

Obstacles diffraction (Chapters IV and V)

Limited flat earth diffraction (Chapters III and VII)

Surface absorption (Chapters VI and VII)

Atmospheric propagation (Appendix C)

Aircraft
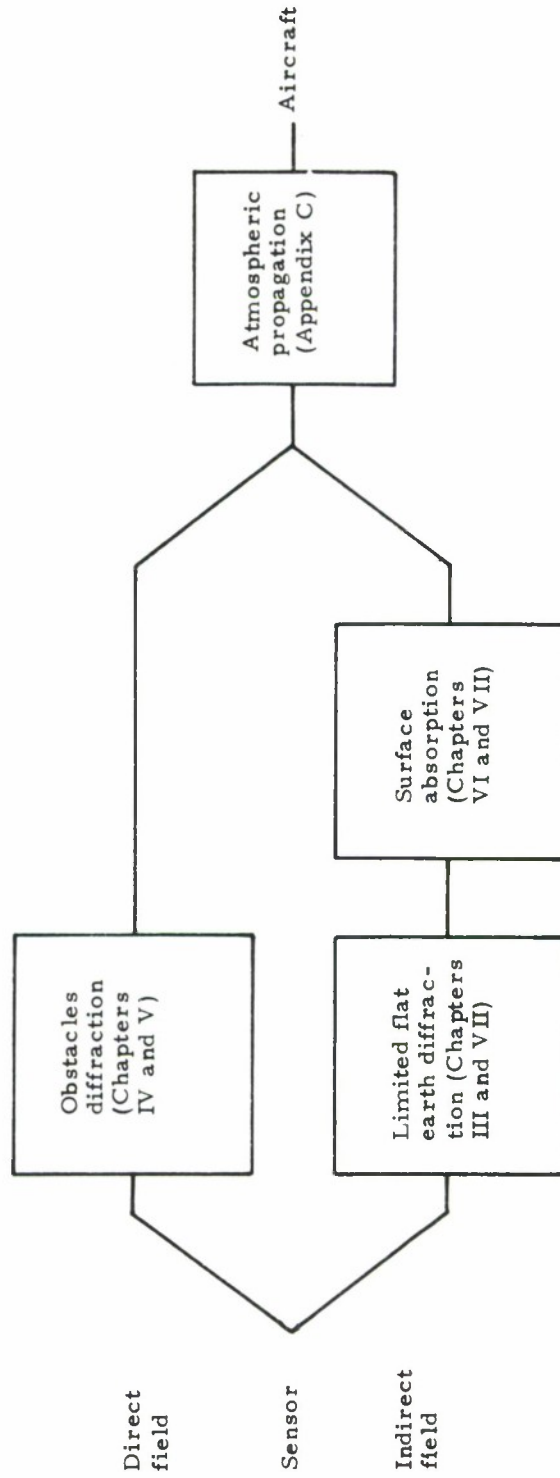
Fig. 2. Organization of technical note.

II. DIFFRACTION IN THE ENVIRONMENT

In this chapter a summary is given of the effect of an aperture on a propagating field; the approach used is based on Fourier optics [Ref. 1]. In succeeding chapters the results are specialized to different cases encountered in various DABS environments.

In a number of cases of interest, the field radiated by an antenna is modified by a reflecting surface or an obstacle. Obstacles in the path of the direct radiation can be modeled as opaque apertures; for a sensor at an airport, the limited flat earth can be modeled as an open aperture in the path of a field radiated by an image antenna. The aperture effect becomes significant when the flat area or aperture subtending the sensor antenna field becomes comparable to the area of the first Fresnel zone. This zone is that portion of the area for which the length of the direct path between source and receiver is shorter by half a wavelength than the length of the path between source and receiver. The path difference is a function of the actual width of the aperture and its relative position with respect to the source and the receiver.

Fresnel Approximation

Consider a two-dimensional field of arbitrary phase and amplitude, $\overline{U}_1(z_1, y_1)$, illuminating the aperture at the source as shown in Fig. 3. Then the received field $\overline{U}_0 (x_0, y_0)$ is given by

$$\overline{U}_0(x_0, y_0) =$$

$$\frac{\exp(jKz)}{j\lambda z} \iint_{-\infty}^{\infty} \overline{U}_1(x_1, y_1) * \exp\left(j\frac{\pi}{\lambda z}[(x_0 - x_1)^2 + (y_0 - y_1)^2]\right)dx_1\, dy_1$$

$$\text{for } z^3 >> \frac{\pi}{4\lambda}[(x_0 - x_1)^2 + (y_0 - \dot{y}_1)^2]_{max}. \tag{1}$$

or equivalently by

$$\overline{U}_0(x_0, y_0) =$$

$$\frac{\exp(jKz)}{2j} \iint_{-\infty}^{\infty} \overline{U}_1\left(\sqrt{\frac{\lambda z}{2}}\,\zeta\right.$$

$$\left. + x_0,\ \sqrt{\frac{\lambda z}{2}}\,\eta + y_0\right) \exp\left(j\frac{\pi}{2}\,\zeta^2\right) \exp\left(j\frac{\pi}{2}\,\eta^2\right) d\zeta\, d\eta$$

where $\zeta = \sqrt{\frac{2}{\lambda z}}(x_1 - x_0)$

$$\eta = \sqrt{\frac{2}{\lambda z}}(y_1 - y_0) \qquad . \tag{2}$$
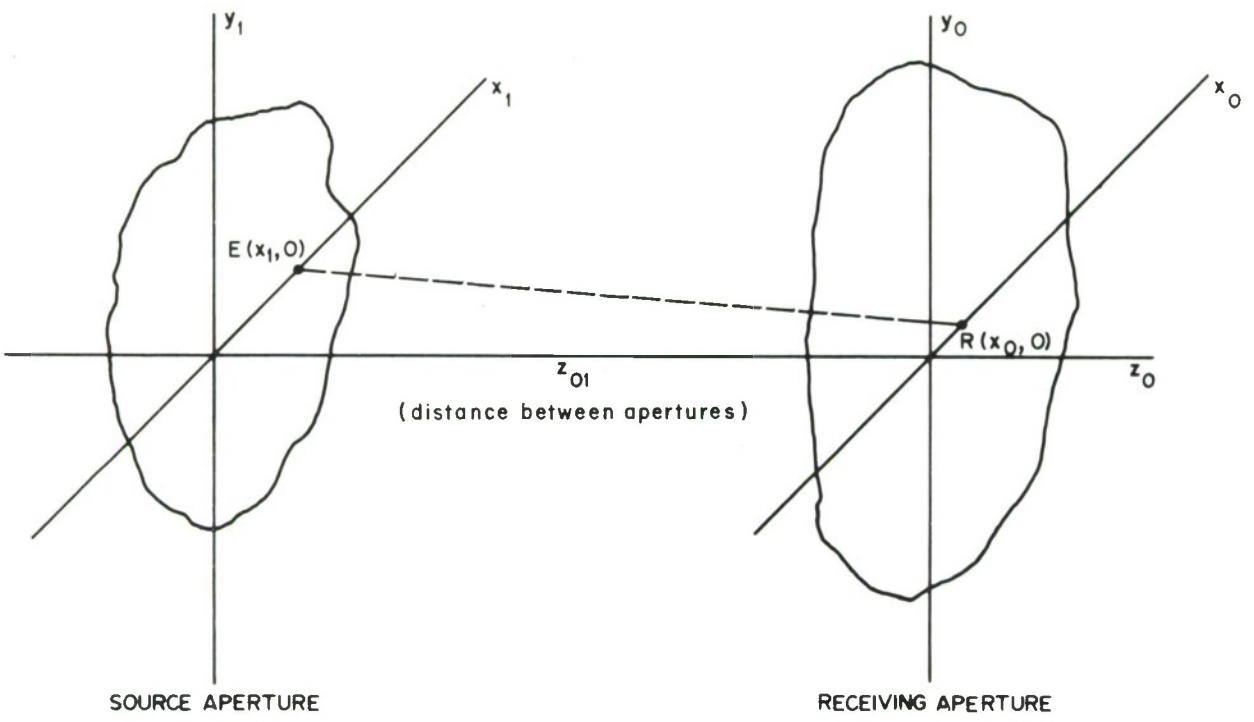
Fig. 3. Source and receiving apertures.

8

In Equation 2, the factor, $\exp(jKz)/2j$, outside the integral introduces a normalizing factor and the phase delay due to the distance between the source and the receiver. The factor, $\exp\left(j\,\frac{\pi}{Z}\,\zeta^2\right)$, within the integral introduces the relative phase delay incurred by the element $d\zeta\,d\eta$ of the source at (ζ, η) due to its **x** coordinate and similarly $\exp\left(j\,\frac{\pi}{Z}\eta^2,\right)$ due to its y coordinate. These phase delays correspond to the separation between the source aperture and the receiving aperture. The validity of the latter observation is readily seen by examining Fig. 3. The path difference (PD) between RE, the distance connecting a receiving point R, to an arbitrary point E on the source aperture, and Z_{01} the distance between the apertures, is given by:

$$PD = RE - Z_{01}$$

$$= \sqrt{(x_1 - x_0)^2 + z^2} \quad -Z_{01}$$

$$\approx 1/2\,\frac{(x_1 - x_0)^2}{Z_{01}}$$

$$\text{for } Z_{01} >> |x_1 - x_0| \quad .$$

Substituting for ζ^2 its value in terms of the cartesian coordinates we have

$$\exp\left(j\,\frac{\pi}{Z}\,\zeta^2\right) = \exp\left(j\,\frac{2\pi}{\lambda}\,*\,PD\right)$$

9

which indeed is the relative phase delay mentioned above. In essence, the Fresnel approximation given in equations 1 and 2 is the vector sum of the incremental source elements with an approximation for the phase delay incurred by the different elements due to their different path length to the receiving point.

In calculating relative field strength, it is not essential to know the true phase of a field; Equation 2 could be replaced by Equation 3

$$U_0(x_0, y_0) = \frac{1}{2j} \int\!\!\int U_1\left[\sqrt{\frac{\lambda z}{2}}\ \zeta + x_0,\ \sqrt{\frac{\lambda z}{2}}\ \eta + y_0\right]\ \exp\!\left(j\frac{\pi}{2}\ \zeta^2\right)\exp\!\left(j\frac{\pi}{2}\eta^2\right)\,d\zeta\ d\eta.$$

(3)

Equation 3 ensures that the received field $U_0(\ )$ is equal to the source field $U_1(\ )$ if the latter is a uniform plane wave.

A case of special interest is that in which the source is uniform, of unity magnitude, and extending between y_L and y_H in the y ordinate, and x_L and x_H in the x ordinate. Then the received field $U_1(\ )$ will be given by

$$U_0(x_0, y_0) =$$

$$\frac{1}{2j} \int_{\zeta_1}^{\zeta_2} \exp\!\left(S\frac{\pi}{2}\ \zeta^2\right)d\zeta \int_{\eta_1}^{\eta_2} \exp\!\left(j\frac{\pi}{2}\ \eta^2\right)d\eta$$

10

with

$$\xi_2 = \sqrt{\frac{2}{\lambda z}} \, (x_h - x_o)$$

$$\xi_1 = \sqrt{\frac{2}{\lambda z}} \, (x_1 - x_o)$$

$$\eta_2 = \sqrt{\frac{2}{\lambda z}} \, (y_h - y_o)$$

$$\eta_1 = \sqrt{\frac{2}{\lambda z}} \, (y_1 - y_o) \qquad . \tag{4}$$

In Equation 4 the two-dimensional integral is decoupled into two similar integrals. It is possible to evaluate each by using tabulated standard Fresnel integrals defined as:

$$C(\alpha) = \int_0^{\alpha} \cos\left(\pi \, \frac{t^2}{2}\right) dt$$

$$S(\alpha) = \int_0^{\alpha} \sin\left(\frac{\pi \, t^2}{2}\right) dt \qquad . \tag{5}$$

Use of Equation 5 in Equation 4 gives for the received field:

$$\overline{U}(x_0, y_0) = \frac{1}{2j} \left(\left(C(\xi_2) - C(\xi_1)\right) + j\left(S(\xi_2) - S(\xi_1)\right)\right) *$$

$$\left(\left(C(\eta_2) - C(\eta_1)\right) + j\left(S(\eta_2) - S(\eta_1)\right)\right) \qquad . \tag{6}$$

11

A graphical representation of the above Fresnel integrals, known as the Cornu spiral, is given in Fig. 4.

By a simple transformation of Equation 1 or its equivalents, it is possible to compute the effect of an aperture between a source and a receiver when both are at finite distances from the aperture. From Fig. 5 the path difference PD between the direct path SR connecting the source to the receiver and SPR, the path passing through the point P in the aperture is given by:

$$PD = \sqrt{(W^2 + Z_S{}^2)} - Z_S + \sqrt{W^2 + Z_R} - Z_R$$

$$\simeq 1/2 \ W^2 \left[\frac{1}{Z_S} + \frac{1}{Z_R} \right]$$

$$\text{for } W << Z_S, \ Z_R \qquad .$$

This implies that in Equation 1 (or its equivalent equations) an effective aperture distance z is given by:

$$\frac{1}{z} = \frac{1}{z_S} + \frac{1}{z_R} \tag{7}$$

where

z_S is the distance of the source from the aperture.

z_R is the distance of the receiver from the aperture.
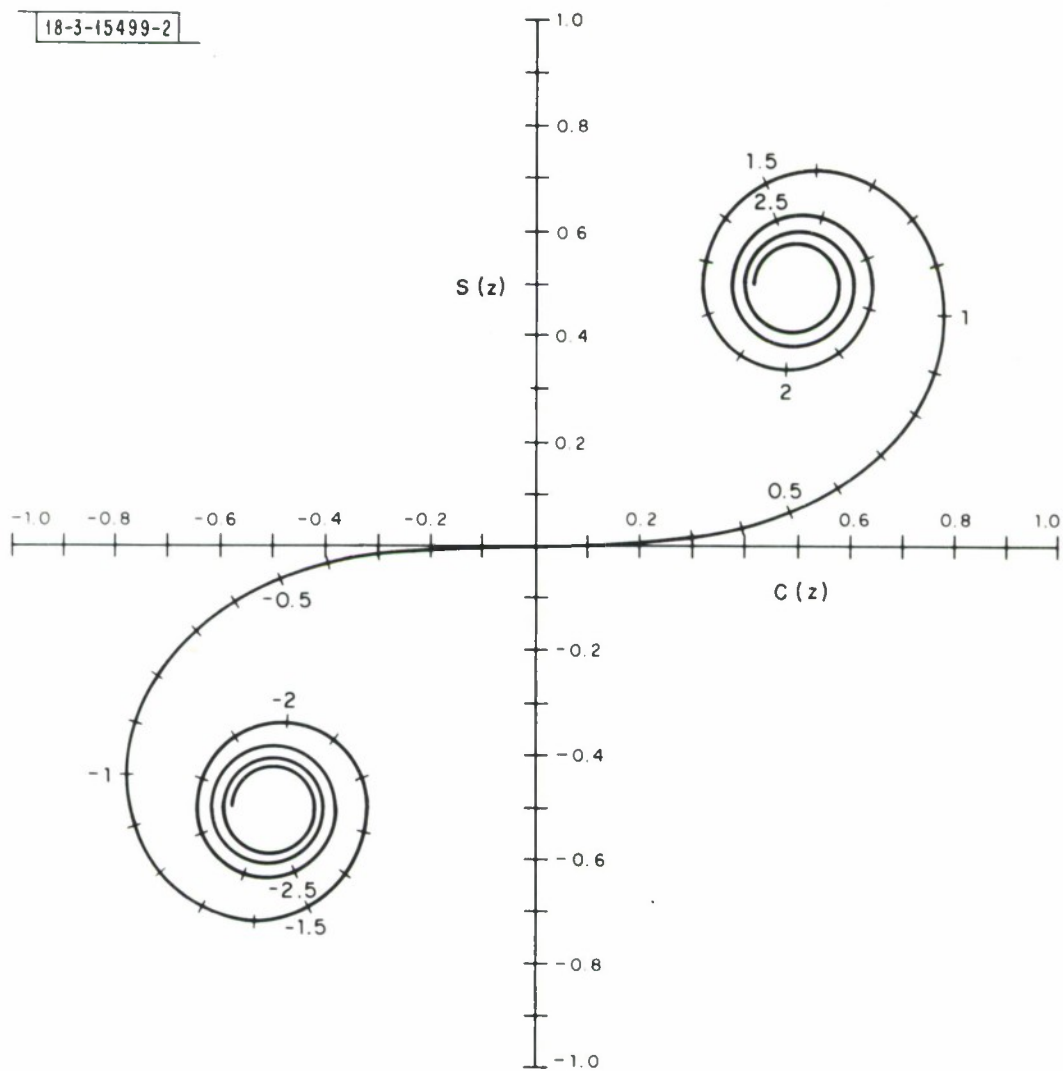
Fig. 4. Representation of Fresnel integrals (Cornu spiral).
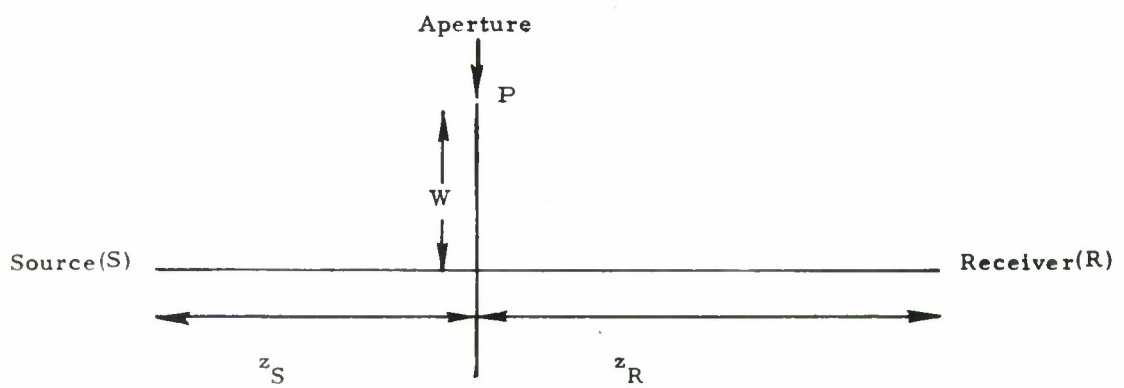
Fig. 5. Relative position of source and receiver from the aperture

Another point of interest is that in the case where the aperture is actually a shield with the other parts open to field transmission, examination of Equation 5 shows that

$$\overline{U}_0(x_0, y_0) = 1 - \frac{1}{2j} \int_{\zeta_1}^{\zeta_2} \int_{\eta_1}^{\eta_2} e^{j\frac{\pi}{2}\zeta^2} e^{j\frac{\pi}{2}\eta^2} d\zeta \, d\eta \qquad (8)$$

with the same definition of variables as in Equation 4. Equation 8 is the complement of Equation 4.

III. LIMITED FLAT SURFACE REFLECTION

A sensor at an airport is typically surrounded by airport grounds and runways that are flat, which, in turn, are surrounded by a built-up area. If the built-up area is assumed to scatter energy randomly, the sensor is then in effect surrounded by only a flat reflecting surface that is limited in range. A simplified model representing this situation is shown in Fig. 6. The field reflected from this limited flat surface is quite different from that corresponding to a flat surface extending to infinity. In this study it has been convenient to designate the ratio of the former field to the latter field by a modification factor $\overline{K}$. The character of $\overline{K}$ is reported in this chapter.

Figure 7 shows a vertical plane including the antenna. As shown in this figure, the antenna image is a virtual source for the reflected field. The antenna image sees an open aperture extending from point F to the vertical axis. The width of the aperture in azimuth is assumed to be wide enough so as to accommodate the narrow beam of the antenna. The aperture is nonuniformly illuminated in elevation as the antenna gain varies with elevation angle. Initially we assume the antenna gain to be constant in elevation. The effect of antenna gain variation in elevation on K will be discussed in Appendix A.

The above assumptions reduce the problem of characterizing K to that of characterizing the diffraction pattern created by such an open aperture. The aperture is uniformly illuminated and one-dimensional extending from F to the vertical axis with a center axis formed by the line connecting the antenna image

16
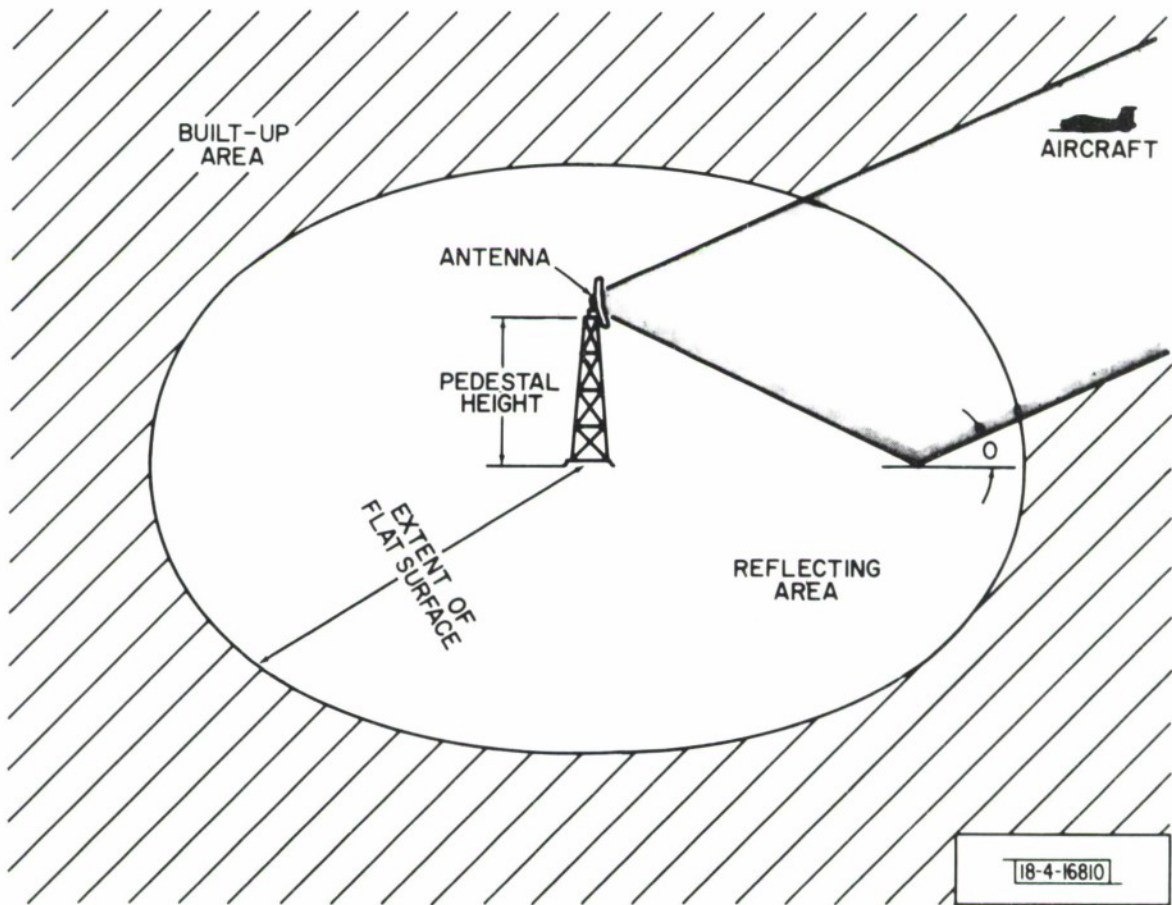
Fig. 6. Model of the sensor at an airport.

APERTURE SEEN BY
ANTENNA IMAGE

OPTICAL PATH

AIRCRAFT

ANTENNA
HEIGHT =
H ft

REFLECTING

O

F

NONREFLECTING

ANTENNA
IMAGE

X

EXTENT OF REFLECTING
SURFACE = d
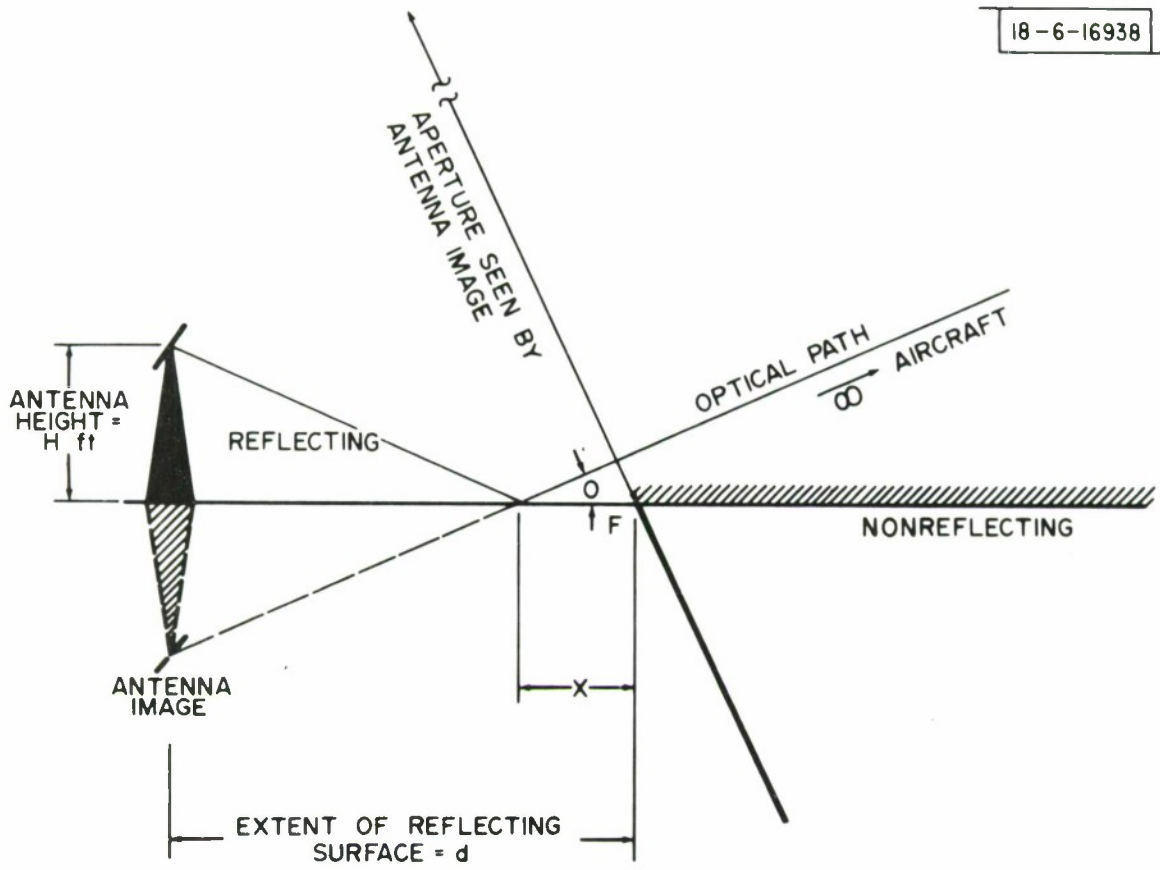
Fig. 7.   Vertical plane cut of the sensor in an airport model.

with the aircraft as shown in Fig. 7. The parameters of Equation 4 corresponding to the present case are:

$$\eta_2 = \infty$$

$$\eta_1 = -\infty$$

$$\eta_2 = \infty$$

$$\eta_1 = \sqrt{\frac{2}{\lambda * z}} * (y_1 - y_0)$$

with

$$z = \frac{h}{\sin \theta} + \left(d - \frac{h}{\tan \theta}\right) * \cos \theta$$

$$y_1 - y_0 = \left(\frac{h}{\tan \theta} - d\right) * \sin \theta$$

where

      h is the antenna height.

      d is the extent of flat earth from the sensor.

      θ is the elevation of aircraft in radians.

19

If

$$d >> h$$

$$\theta << 1$$

then

$$\eta_1 = \sqrt{\frac{2}{\lambda * d}} \; * \; (h - d * \theta) \qquad\qquad (9\text{-}a)$$

and we have for K

$$K(h, d, \theta, \lambda)$$

$$\frac{1}{\sqrt{2j}} \int_{\eta_1}^{\infty} \exp\!\left(j * \frac{\Pi}{2} * \eta^2\right) d\eta \qquad . \qquad\qquad (9\text{-}b)$$

The integral given in Equation 9-b is tabulated in mathematical hand-books. The magnitude and phase of K is given in Figs. 8 and 9 as a function of $\left|\eta_1^2\right| *$ sign (η_1). It is to be noted that the maximum value of $\left|K\right|$ as shown in Fig. 8 is 1.17. This occurs at $\eta = -1.26$. Another feature of the magnitude of K is that its value at other peaks, as shown in Fig. 8, decreases as η_1 decreases in value.
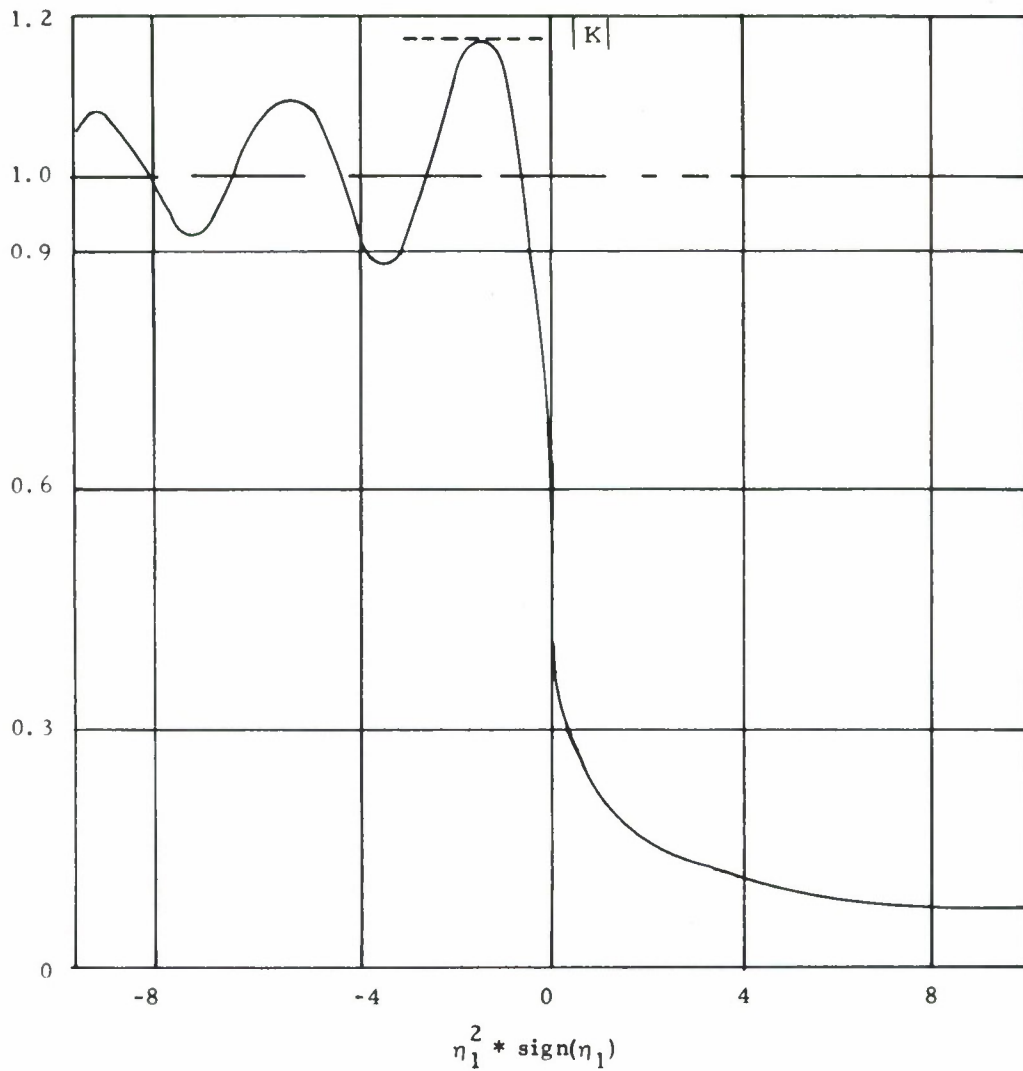
Fig. 8. The magnitude, $|K|$, of the modification factor due to limited flat earth reflection.
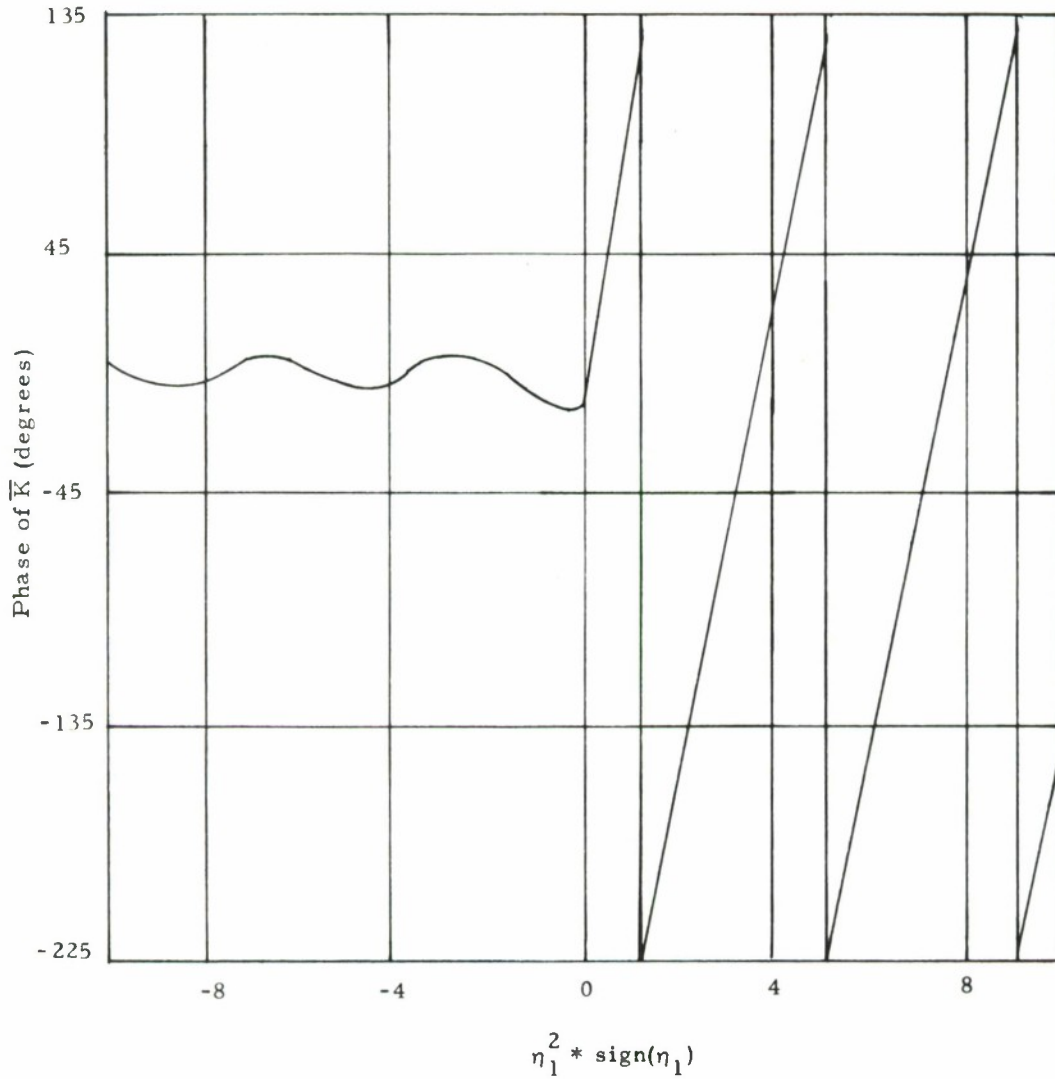
Fig. 9. The phase of $\overline{K}$, the modification factor due to limited flat earth reflection.

For purpose of illustration, consider the following:

|	
Antenna height	50 feet
Reflecting surface extent	8,000 feet
Wave length, λ	1 foot
Antenna elevation pattern	Mod ASR has a cutoff of 1.1 dB/deg, and a free space gain of 23 dB at horizon
Dry earth condition	See Chapter VI

The modification factor $\overline{K}$ is computed as a function of aircraft elevation using equation 9 and is given in Figs. 10 and 11. The vertical lobing of the antenna pattern is shown in Fig. 12. The equations used in the computation are given below. Also shown in Fig. 12 is the lobing pattern corresponding to flat earth extending to infinity. In computing the lobing for flat earth, the equations below are used with K = 1. It is interesting to note that the null for the limited flat earth is deeper at 0.8 degree elevation than the one occurring at 0.4 degree elevation. Also the null occurring at 0.8 degree elevation is deeper than the null corresponding to flat earth.

Uplink field	=	Direct field + reflected field
Direct field	=	$10^{(G(\theta)/20)}$
Reflected field	=	$10^{(G(-\theta)/20)} * 10^{(-\theta/20)} * \left| K(75, 12000, \theta, 1) \right|$
Phase of reflected field compared to direct field	=	$180 + 360 * 150 * \sin\theta$ − phase of $K(75, 1200, \theta, 1)$

where

θ is elevation angle (degrees)

G( ) is gain of the antenna in (dB).

23
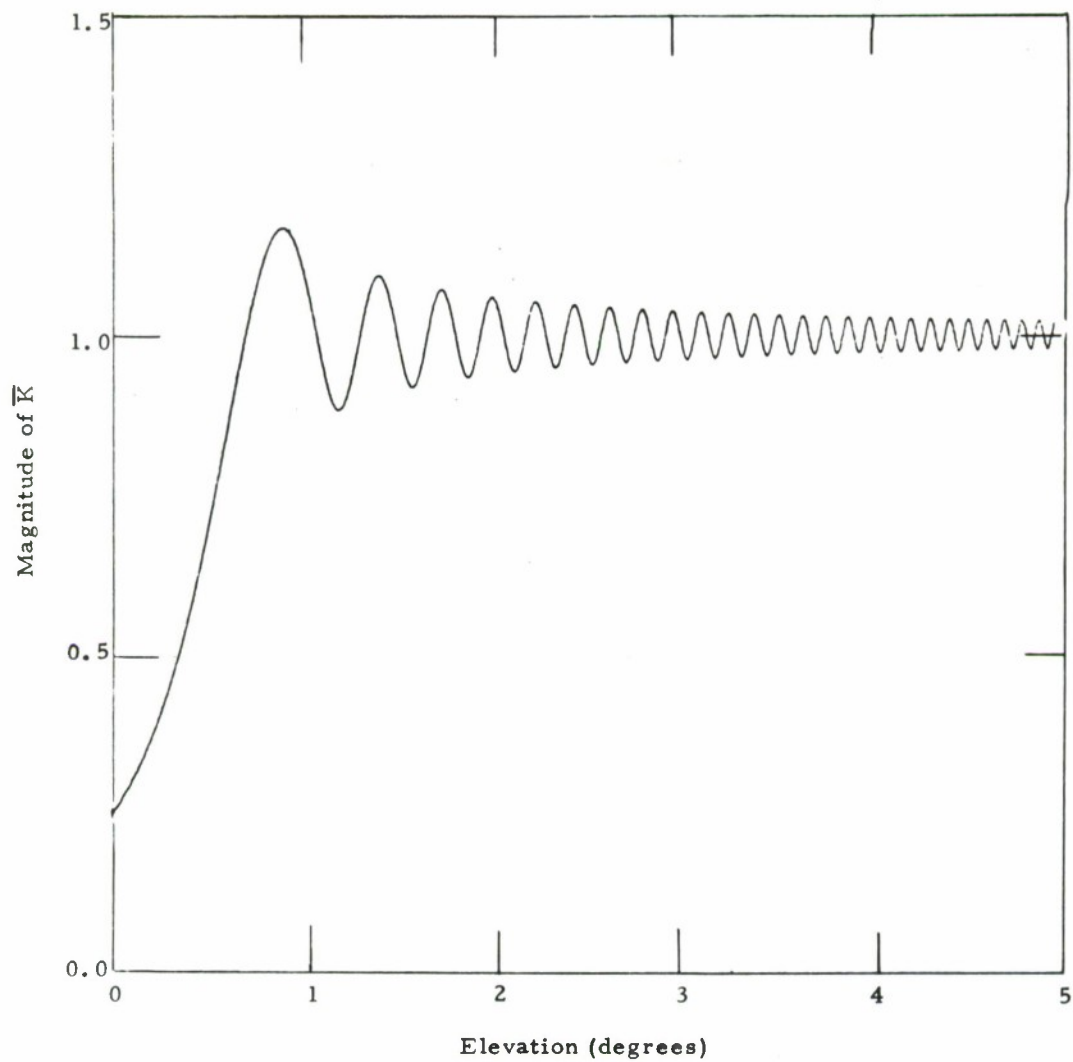
Fig. 10. Magnitude of the modification factor $\overline{K}$ due to limited flat earth reflection for a 50-ft antenna height; limited flat earth extending to 8000 ft, and $\lambda = 1$ ft.
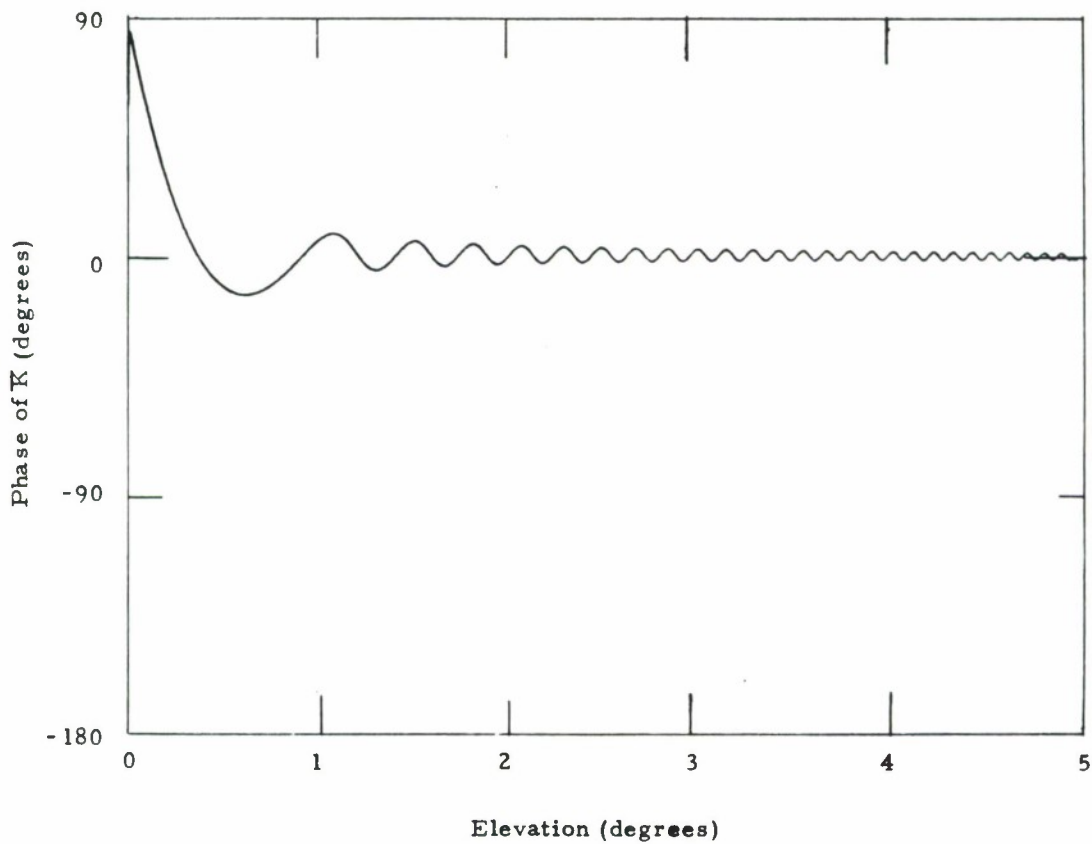
Fig. 11. Phase of the modification factor , $\overline{K}$, due to limited flat earth reflection for a 50-ft antenna height; limited flat earth extending to 8000 ft, and λ = 1 ft.
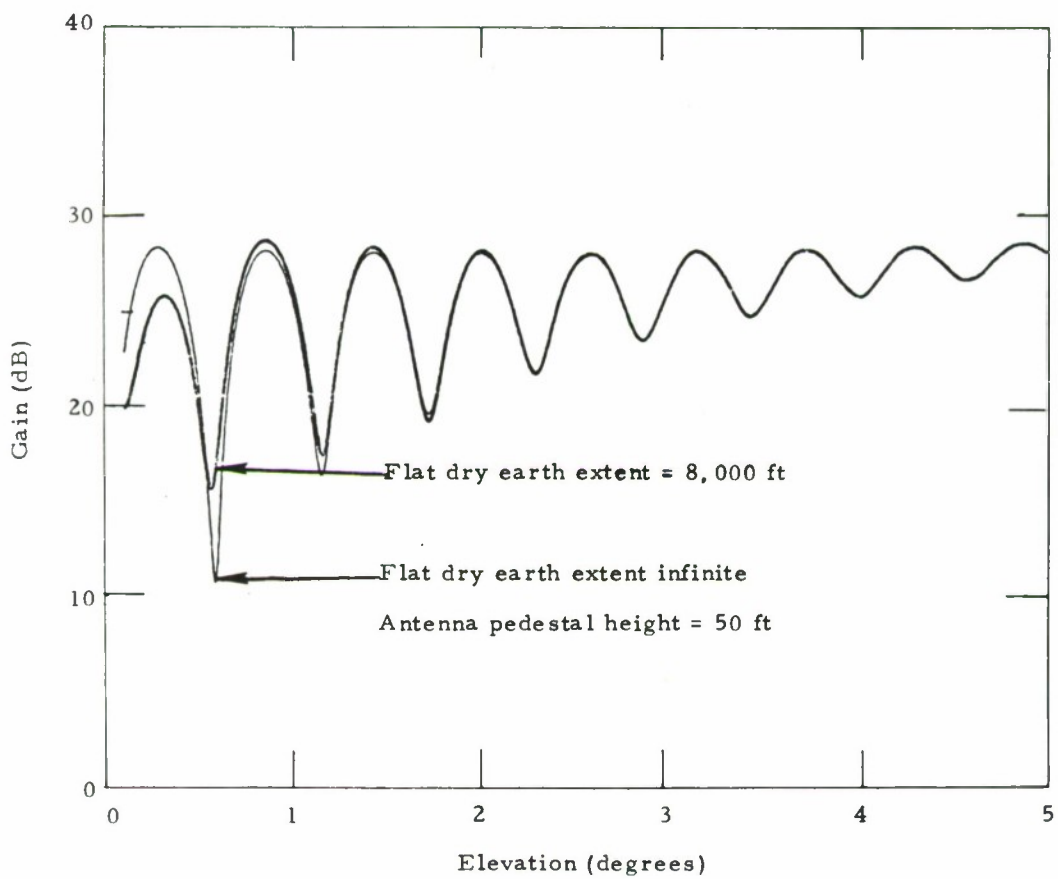
Fig. 12. Lobing of Modified ASR antenna.

The chart shows Gain (dB) on the vertical axis from 0 to 40, and Elevation (degrees) on the horizontal axis from 0 to 5. Labels within the chart read:

Flat dry earth extent = 8,000 ft

Flat dry earth extent infinite

Antenna pedestal height = 50 ft

IV. SHADOW CAST BY AN OBSTACLE

This chapter covers fades occurring in the shadow of obstacles such as buildings between the sensor and the aircraft. (See Fig. 13.)

The problem is studied under the assumption that the obstacle is isolated and that there are no other obstacles adjacent to or behind it. The obstacle is represented by the geometry of Fig. 14. For a source field with unity magnitude the received field U_r, excluding path loss, is given by:

$$U_r = 1 - \frac{1}{2j} * \left\{ \left(C(\alpha_2) - C(\alpha_1) + j \left(S(\alpha_2) - S(\alpha_1) \right) \right) * \right.$$

$$\left. \left(C(\beta_2) - C(\beta_1) + j \left(S(\beta_2) - S(\beta_1) \right) \right) \right\} \tag{10}$$

where

$$\alpha_1 = \sqrt{\frac{2}{\lambda}} * \sqrt{\frac{1}{R_1} + \frac{1}{R_2}} * W_1$$

$$\alpha_2 = - \sqrt{\frac{2}{\lambda}} * \sqrt{\frac{1}{R_1} + \frac{1}{R_2}} * W_2$$

$$\beta_1 = - \infty$$

$$\beta_2 = \frac{2}{\sqrt{\lambda}} * \left[R_1 * \left(\frac{\epsilon_1^2}{2} - \frac{\epsilon_2^2}{2} \right) + R_1 * (\epsilon_2 - \epsilon_1) * \epsilon_2 \right.$$

$$\left. - \frac{R_1^2 * (\epsilon_2 - \epsilon_1)^2}{2 * R_2} \right]^{1/2}$$

27

18-4-16846

OBSTACLE
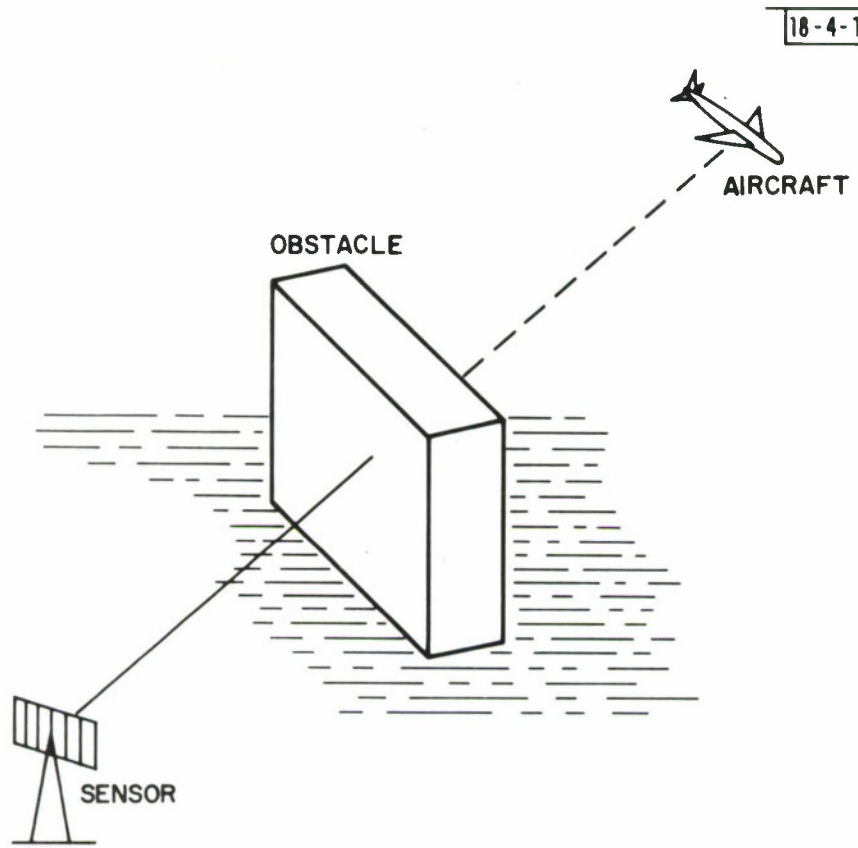
AIRCRAFT

SENSOR

Fig. 13. Shadow cast by obstacle between sensor and aircraft.

18-4-16847

AREA 1
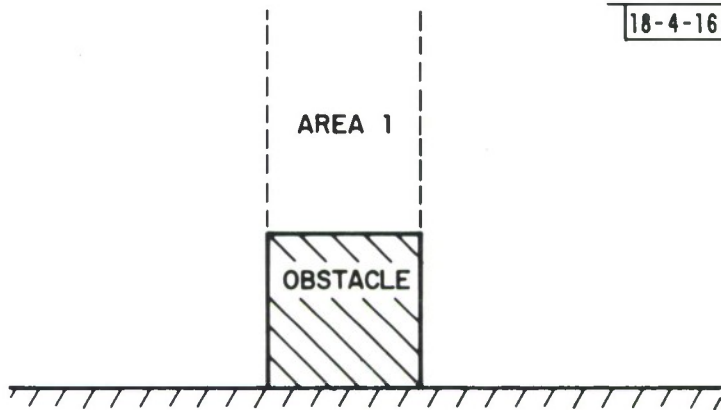
OBSTACLE

Fig. 14-a. Obstacle as seen from sensor.
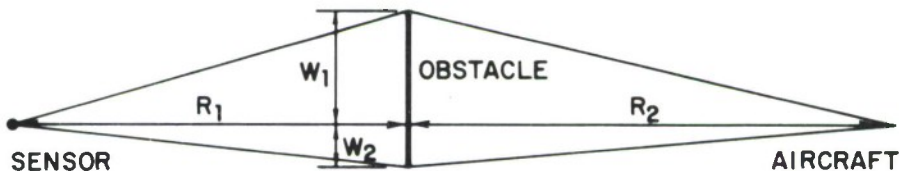
14-b. Plan view.
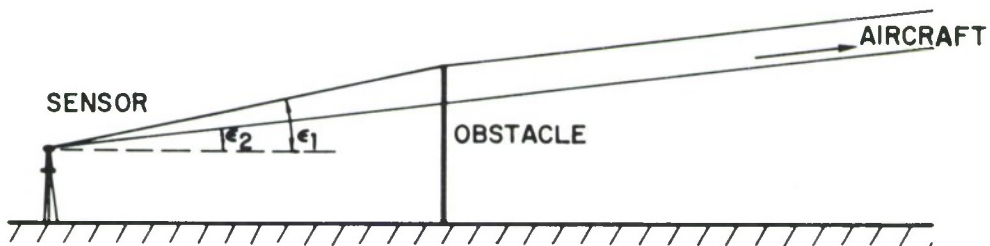
14-c. Vertical view.

R_1 is range of obstacle from sensor

R_2 is range of aircraft from obstacle

W_1 is distance from one edge of the obstacle to
   the line joining the aircraft to the sensor

W_2 is the distance from the other edge of the obstacle
   to the line joining the aircraft and the sensor

ϵ_1 is elevation of obstacle top from the sensor (radians)

ϵ_2 is elevation of the aircraft from the sensor (radians)

and C( ) and S( ) are defined in Equation 5.

The field contributed by area 1 in Fig. 14-a is reduced by 20 dB or more relative to free space gain due to shadowing if

$$\beta_2 > 2.08 \quad .$$

For an aircraft range that is large compared to obstacle range, this condition corresponds to

$$\epsilon_2 < \epsilon_1 - \frac{2\lambda}{\sqrt{R_1}} \quad . \tag{11}$$

If condition 11 is satisfied, then Equation 10 is simplified to correspond to a one-dimensional diffraction problem; namely, the received field U_r strength will be given by:

$$U_r = 1 - \frac{1-j}{2} \left\{ C(\alpha_2) - C(\alpha_1) + j \, (S(\alpha_2) - S(\alpha_1)) \right\} \qquad (12)$$

with

$$\alpha_1 = \sqrt{\frac{2}{\lambda R}} * W_1$$

$$\alpha_2 = - \sqrt{\frac{2}{\lambda R}} * (W - W_1)$$

where

W_1 is the distance of the radial joining the sensor to the target

from one edge of the obstacle

R is the range of the obstacle, and the aircraft is at very long range

W is the width of the obstacle.

Figure 15 illustrates the character of the fade for a target with a $W/\sqrt{R\lambda} = 1.517$. Two special values of the fade are to be noted: one is the deepest fade which, in the present example, is 18.5 dB with respect to free space gain, and the other is the fade that is midway between the two edges of the obstacle which is 8.5 dB with respect to free space gain. These two fades are plotted as a function of $W/\sqrt{R\lambda}$ in Fig. 16. From this figure, it may be noticed that if

$$W/\sqrt{R\lambda} > 1.0 \qquad (13)$$

31

the fade midway in azimuth is deeper than 6 dB. This provides a simplified criteria for a significant fade in its shadow. One consequence of Equation 13 is that obstacles casting significant fade in their shadows have a minimum azimuth angle with respect to the sensor that decreases with the range of the obstacle.
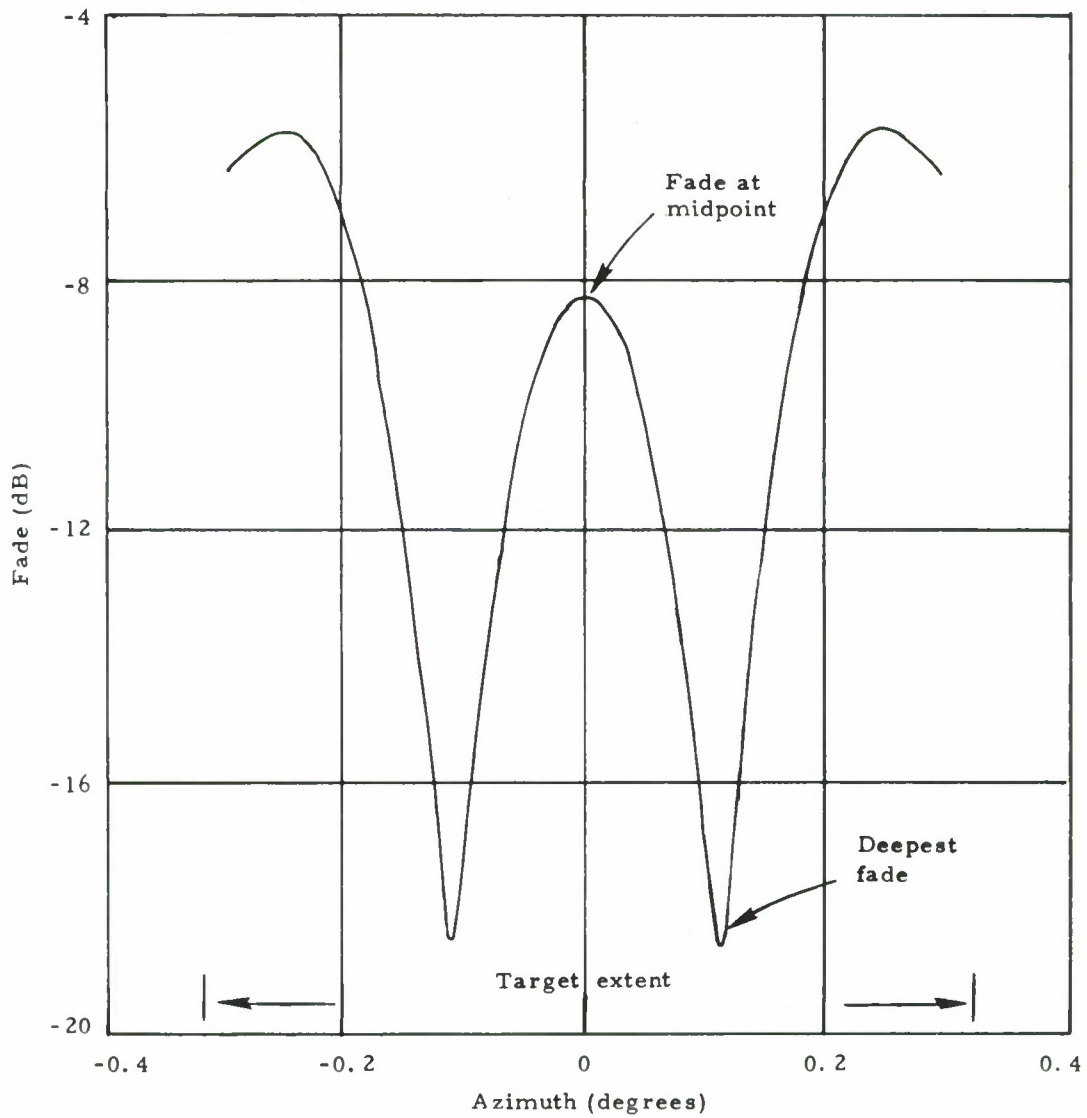
Fig. 15. Fade cast by shadow of obstacle with $W/\sqrt{R\lambda} = 1.517$ (obstacle corresponds to Prudential building as seen from Logan Airport at DABS frequency).
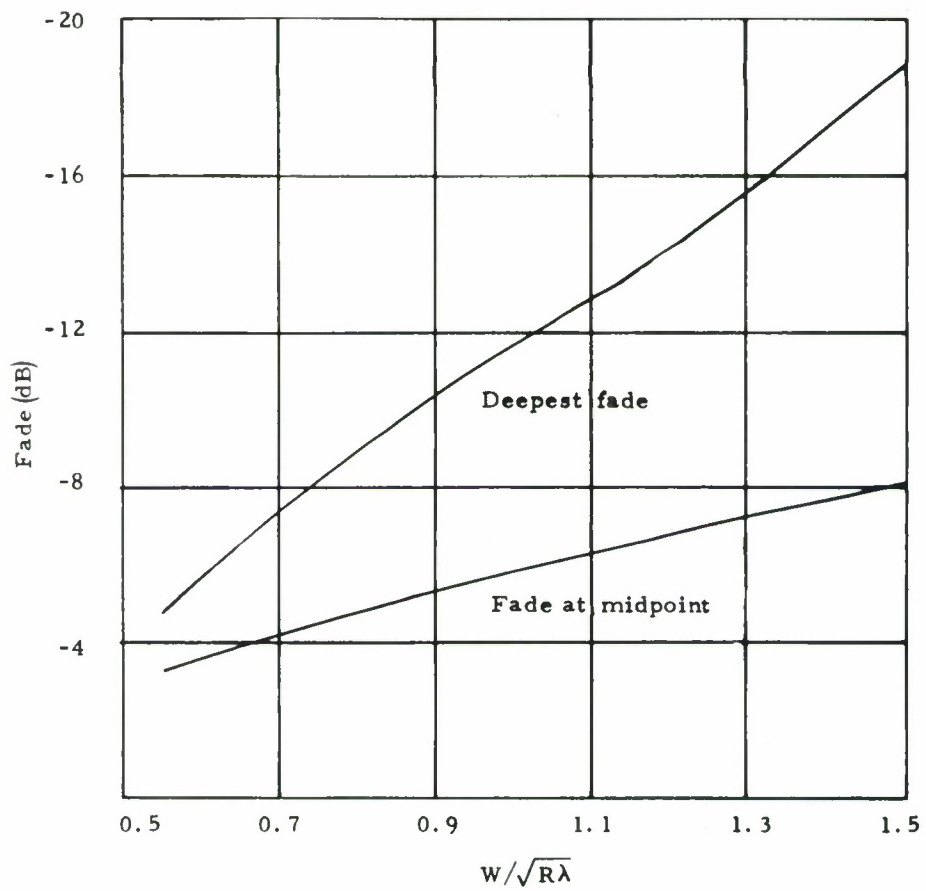
Fig. 16. Fade in shadow as a function of obstacle range and width; receiver is assumed to be at very long ranges.

V. MULTIPLE EDGE DIFFRACTION

Fade, due to multiple edge diffraction, is discussed in this chapter. Such fades are of interest at an enroute sensor installed in a hilly environment where the direct field skirts hilltops at grazing angles. These hilltops act as a succession of knife edge apertures, each attenuating the field. A similar situation occurs when a field that is reflected from a patch of flat surface is diffracted by the top of a ridge. Here the source is the antenna image; the first aperture is the patch of flat surface, and the second aperture is the knife edge corresponding to the ridge top.

A pictorial description of the multiple aperture problem is given in Fig. 18 where each aperture is one-dimensional with semi-infinite extent.

The field $U_{n+1}(x_{n+1})$ existing on top of edge $n + 1$ is related to the field $U_n(x_n)$ existing at edge n by the following equation:

$$U_{n+1}(x_{n+1}) = \frac{1}{j\lambda y_{n+1}} \int_{n_1}^{\alpha} \overline{U}(x_n) \exp\left(\frac{j\pi}{\lambda Y_{n+1}} (x_{n+1} - x_n)^2\right) dx_n$$

(14)

where

x_i is the vertical coordinate of the top of hill i, and h_i is the height of the hilltop.

Equation 14 is a special case of Equation 1 with the constant phase delay outside the integral omitted.
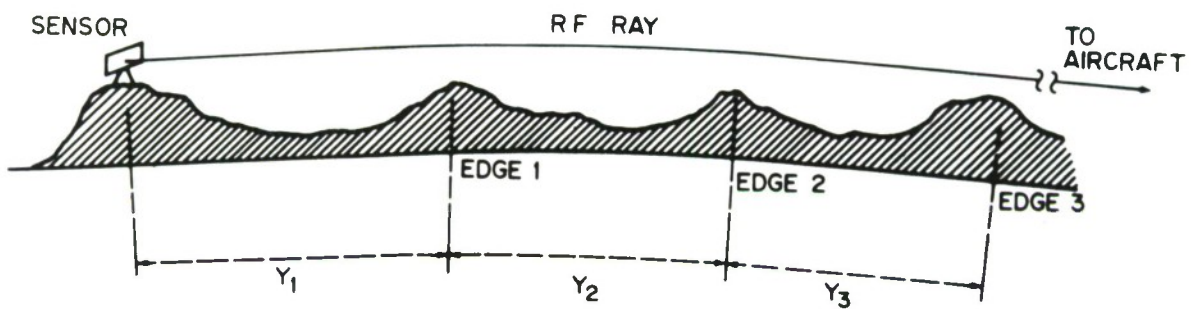
Fig. 17.   Multiple edge diffraction.

Repeated application of Equation 14 to account for the diffraction of each of the edges leads to the following equation for the received field.

$$U_r = \frac{1}{\Pi_i (j \lambda y)} \int_{n_1}^{\infty} \exp\left[\left(\frac{x_1^2}{y_1} + \frac{(x_2 - x_1)^2}{x_2}\right) * \frac{\pi}{\lambda}\right] dx_1 \int_{h_2}^{\infty} \exp\left[\frac{(x_3 - x)^2}{y_3} * \frac{\pi}{\lambda}\right] dx_2 *$$

$$----- \int_{h_{i-1}}^{\infty} \exp\left[\frac{(x_i - x_{i-1})^2}{y_i^2} * \frac{\pi}{\lambda}\right] dx_{i-1} *$$

$$\int_{h_i}^{\infty} \exp\left[\frac{(x_i)^2}{y_{i+1}} * \frac{\pi}{\lambda}\right] dx_i \qquad . \tag{15}$$

Equation 15 involves an i dimensional integral for which no closed form is available. The problem was investigated in more detail for a double knife edge as depicted in Fig. 18. The solution is given in terms of a double integral corresponding to Equation 15. A linear transformation is applied to the variables of integration so as to give the result in terms of two Fresnel surface integrals. The Fresnel surface integral G( ) is defined as:

$$G(\rho, \gamma) = \int_S \exp\left(j \frac{\pi}{2} \rho^2\right) ds \tag{16}$$

where S is a wedge, one side of which is bounded by a vertical plane through the origin. The apex of the wedge is a distance ρ from the origin, and the

37
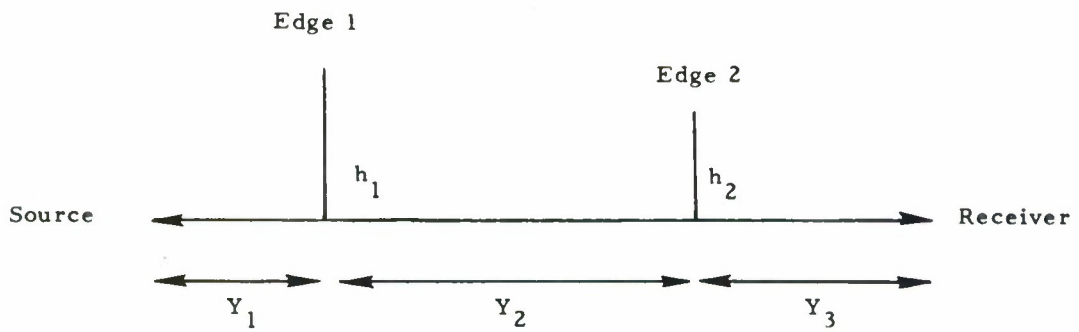
Fig. 18. Definition of variables in the double knife edge probelm.

wedge is γ degrees wide as shown in Fig. 19 . The properties of the Fresnel surface integral are given in reference 3.

The solution of the double knife edge problem [Ref. 2] is given by

$$U_r = \frac{1}{2j} \left[G(\rho_0, \gamma_1) + G(\rho_0, \gamma_2) \right] \tag{17}$$

where

$$\gamma_1 = \tan^{-1} \left[g \sin \alpha / (p - g \cos \alpha) \right] \tag{17-b}$$

$$\gamma_2 = \pi - \alpha - \gamma_1$$

$$\rho_0 = \frac{(p^2 + g^2 - 2 p g \cos \alpha)^{1/2}}{\sin \alpha} \tag{17-c}$$

$$\alpha = \tan^{-1} \left[\frac{Y_2 (Y_1 + Y_2 + Y_3)}{Y_1 * Y_3} \right]^{1/2} \tag{17-d}$$

$$p = \frac{2}{\lambda} \left[\frac{(Y_1 + Y_2 + Y_3)}{Y_1 (Y_2 + Y_3)} \right]^{1/2} * h_1 \tag{17-e}$$

$$g = \left[\frac{2}{\lambda} \frac{(Y_1 + Y_2 + Y_3)}{(Y_1 + Y_2) Y_3} \right]^{1/2} * h_2 \tag{17-f}$$

In Fig. 20, numerical values illustrate the double knife edge diffraction fade, as given by Equation 17, for the case where the tops of the two edges barely touch the line connecting the source with the receiver. The value of fade F, corresponding to U_r in Equation 17, is given for different spacing of the edges Y_1, Y_2, and Y_3 as shown in Fig. 18. From Fig. 20 it may be seen that the fade obtained by assuming the edges to be independently diffracting, i.e., 12 dB, is 30% higher than the actual fade for approximately uniformly

39
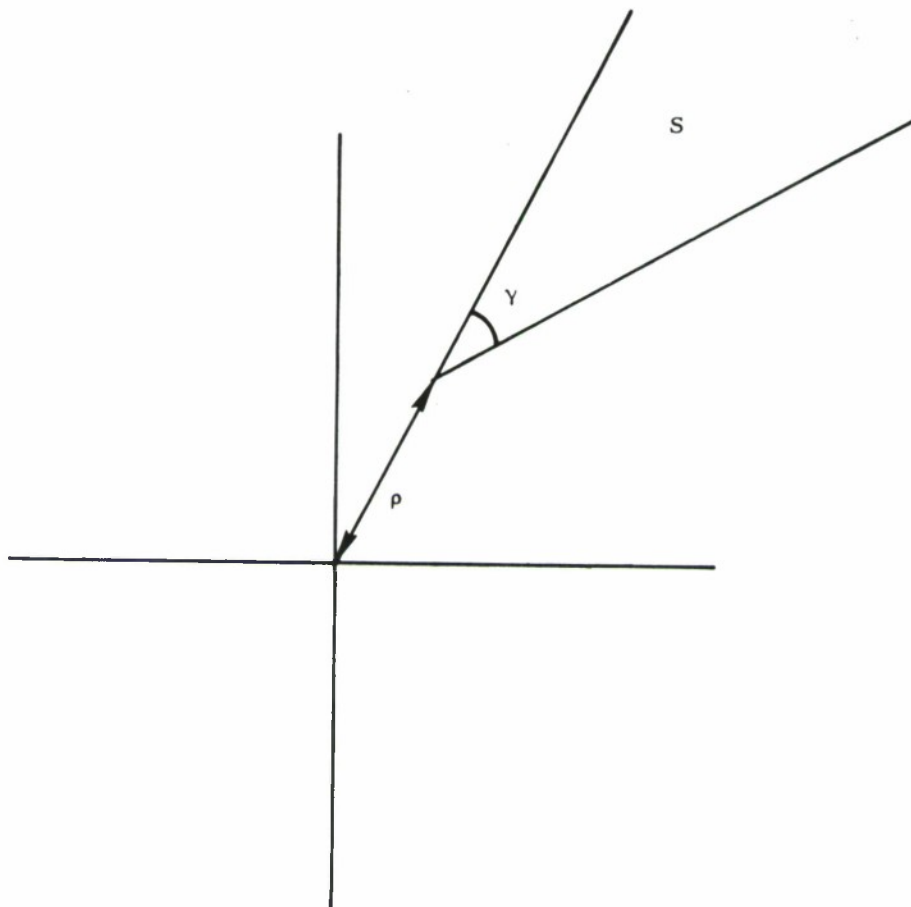
Fig. 19.   Definition of the wedge in the Fresnel surface integral.
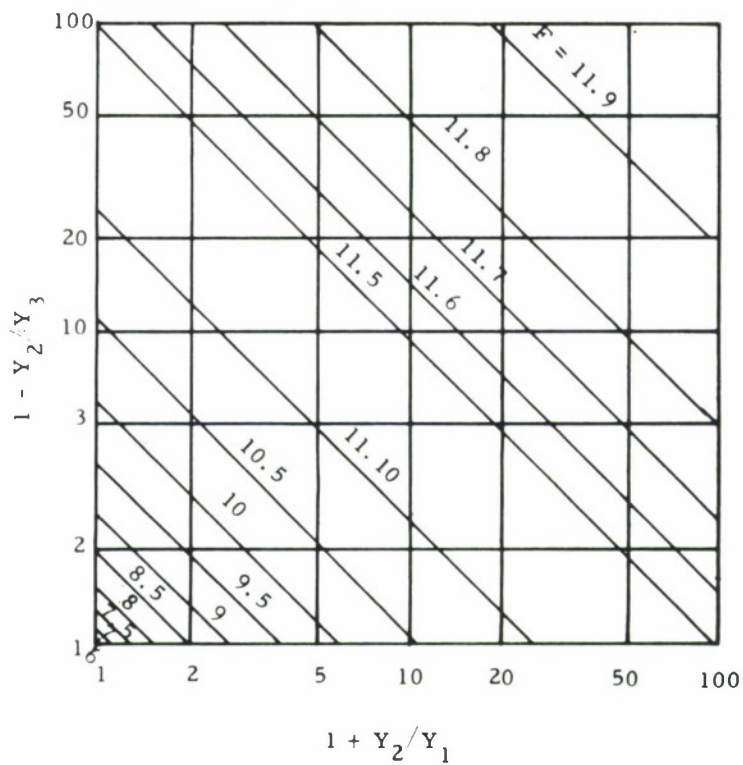
Fig. 20.   Fade due to diffraction over two edges that are at zero-elevation
angles as a function of their spacing, Y_1, Y_2, and Y_3 shown in Fig. 18.

41

spaced hill edges. Considering the problem of diffraction of several hilltops, a 'reasonable' upper bound on the fade is thus given by assuming prominent hilltops to diffract independently. The overestimate in the fade magnitude is partly offset by neglecting diffraction by the minor hilltops. In Fig. 21, the range to the ith hill is R_i, and the height of the hilltop is h_i. Using Equation 2, the single edge attenuation U_i for hill i is given by:

$$\overline{U}_i = \frac{1}{\sqrt{2j}} \int_{\eta_i}^{\infty} \exp\left(j * \frac{\pi}{2} * \eta^2\right) d\eta \tag{18}$$

where

$$\eta_1 = (h_i - h_{i-1} - (R_i - R_{i-1}) * \tan \theta) * \sqrt{\frac{2}{\lambda * (R_i - R_{i-1})}}$$

θ is the elevation angle of the aircraft

R_i is the range to hill i

h_i is the height of hill i

Then $F_{max}(\ )$, the upper bound on total fade in dB produced by all the hills is:

$$F_{max}(\theta) = 20 * \Sigma \log |U_i| \quad . \tag{19}$$

The function $F_{max}(\ )$ has a knee at an elevation angle θ_{knee} where the direct ray is shorter by half a wavelength than the ray passing through one of the hilltops. θ_{knee} is defined by

42

$$\theta_{knee} = \underset{i}{\text{Max}} \ \tan^{-1} \left[\sqrt{\frac{\lambda}{R_i}} + \frac{h_i - H}{R_i} \right] \qquad (20)$$

where

        H is the antenna height.

The elevation angle θ_{knee} denotes the angle at which the grazing null, due to diffraction over hilltops, starts to become significant. For purposes of illustrating the upper bound on grazing fade, consider four hills on a radial from Lincoln Laboratory, with ranges and relative heights with respect to the sensor antenna as follows:

Range (feet)	Relative Height (feet)
35,000	-90
42,500	-130
97,500	-130
107,500	-80

A plot of the grazing null fade for the above hills is given in Fig. 22.

The fade loss due to diffraction over a rounded hilltop tends to be larger than the fade loss over a hill with a knife edge top. This loss increases with increase of radius of curvature. Reference 4 gives the loss over an isolated round top edge as a function of its radius of curvature. These losses are treated in Appendix B of this report.

43
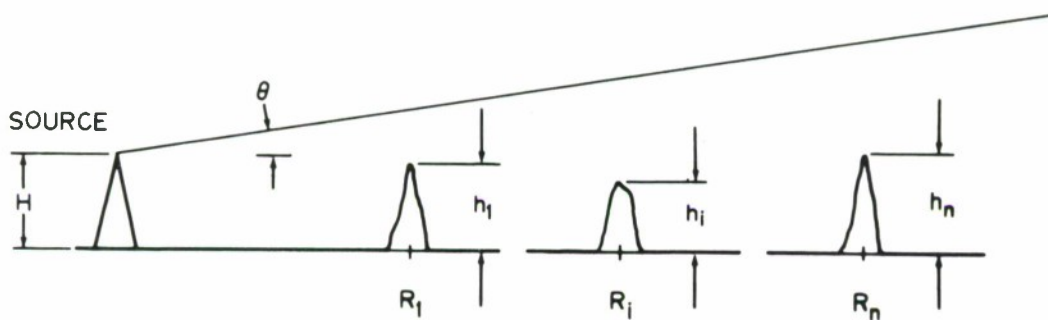
Fig. 21. Several hilltops diffracting the direct ray.
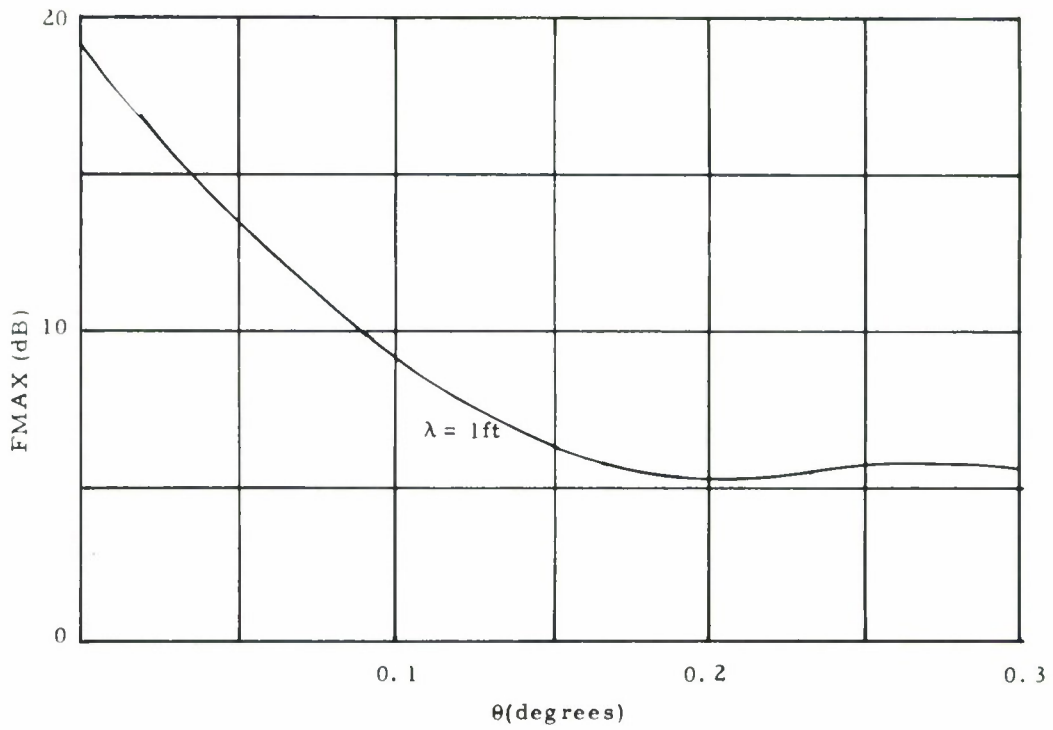
Fig. 22. Grazing angle null fade FMAX due to diffraction by several hills as a function of elevation angle (θ).

VI. FLAT SURFACE REFLECTION COEFFICIENT

This chapter covers the attenuation values to be expected when an RF field is reflected from flat surfaces that have different surface properties, e.g., snow, dry earth. Reflection by such surfaces introduces not only amplitude modification but a phase shift as well. This is caused by mismatch in electrical characteristics between free space and the surface, as well as the granularity of the surface. It is important to characterize this reflection process as it affects the vertical lobing pattern of a sensor antenna located at an airport as depicted in Chapter III.

At RF and polarization utilized by DABS, the reflection phase shift within a few degrees above the horizon is 180 degrees. The amplitude attenuation (dB vs aircraft elevation angle) for several common surface conditions is shown in Fig. 23. These characteristics are essentially straight lines in this region (accuracy better than 3%); their slopes are given in Table 1. If the attenuation of the reflected field (due to antenna cutoff) is combined with that due to surface reflection, then the total attenuation could be attributed to a hypothetical antenna with a cutoff E_C in dB/deg given by:

$$E_C = E_A + E_R/2 \qquad\qquad (21)$$

where

E_A is the antenna elevation pattern cutoff (dB/deg)

E_R is the reflection process absorption (dB/deg).
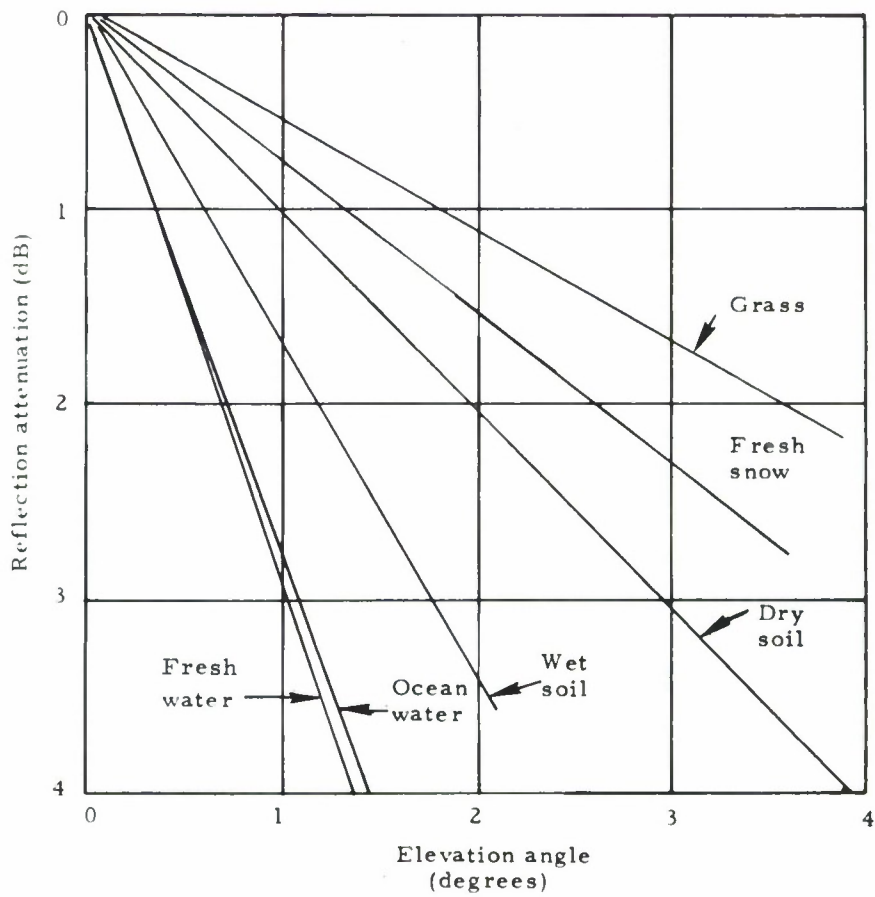
Fig. 23. Attenuation of reflected field by flat surface with different conditions.

TABLE 1

ATTENUATION OF REFLECTED FIELD DUE TO DIFFERENT SURFACE
CONDITIONS

Surface Condition	Reflection Attenuation (dB/deg)
Grass	0.56
Fresh snow	0.77
Dry soil	1.00
Wet soil	1.67
Ocean water	2.66
Fresh water	2.80

The factor of $1/2$ (in the second term of Equation 21) is inserted because the attenuation of the reflected field, with respect to the direct field, varies as the angle between the direct ray and the reflected ray, an angle two times that used in calculating the attenuation due to reflection absorption. Equation 21 may be thought of as establishing a tradeoff between surface condition and antenna elevation pattern underside cutoff. Antenna underside cutoff is important as it is one requirement that determines antenna vertical aperture. A feel for the impact of surface condition on elevation pattern underside cutoff may be gained by noting that with all conditions the same except surface condition, one more dB/deg cutoff is required to maintain the same fade for grass surface condition than for fresh water condition.

VII. EFFECT OF ROUGH TERRAIN ON REFLECTED FIELD

The most desirable terrain is nonflat such as surrounds a sensor when it is located in the country, or as represented by houses and other structures when the sensor is surrounded by a built up area. Nonflat terrain tends to reduce the magnitude of the reflected field. Two processes are involved in such reduction of the reflected field. The first is shadowing, a process that reduces reflection by reducing the amount of terrain that is visible by the sensor . Such an effect may be caused by hilltops or high structures that obstruct the path of the reflected field. The second process is scattering of the reflected field. Figure 24 is an illustration of shadowing. The degree of shadowing increases as the aircraft elevation angle decreases; more hills are then visible between the average terrain and the aircraft. This increase in shadowing also occurs when there are more nearby hills, or their tops are higher above the surrounding terrain. Terrain local roughness scatters the reflected field producing an incoherency in the phase of reflected energy. This reduces the magnitude of the net reflected field as compared to the field reflected from a flat surface. The attenuation of a reflected field increases as the terrain becomes rougher or the elevation angle of the aircraft increases.

Shadowing and scattering help to keep the reflected field at a low level as the elevation angle of an aircraft varies. Shadowing is the predominant mechanism that reduces the field for small elevation angles, while scattering is predominant at higher elevation angles. In analyzing the effect of terrain roughness, it is convenient to decompose the overall nonflat character of the terrain into two categories, thus making it possible to account for its non-stationary character.
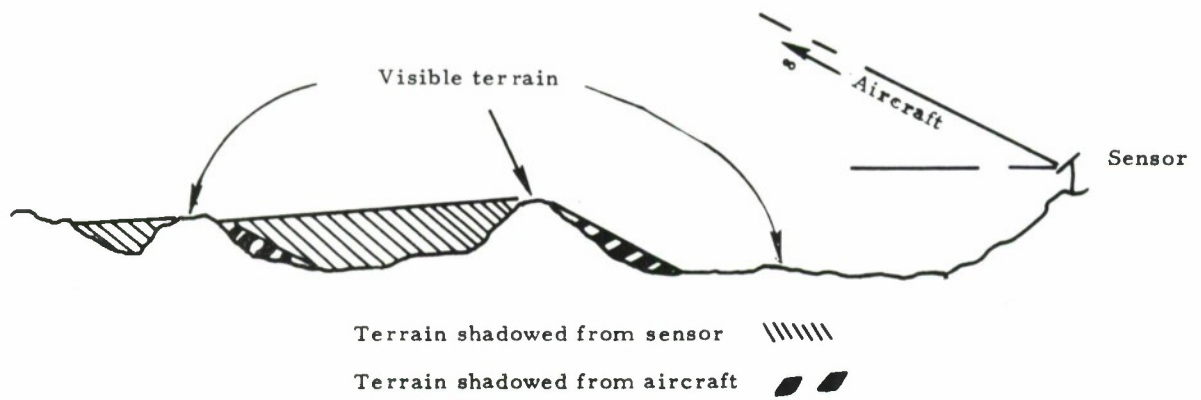
Fig. 24. Shadowing; aircraft is assumed to be at very long range

Shadowing

Shadowing could be assessed computationally using a topographic data base describing the terrain. The terrain contour would be low pass filtered to remove the shadowing due to local roughness, and an aircraft elevation angle assumed and the patches of visible terrain determined. Assuming the patch to be a perfectly flat plane that best fits the visible terrain, calculating the reflected field from each patch would then follow procedures for calculating the reflected field from a limited flat surface as described in Chapter III. Although laborious, this approach is suitable for a case by case study.

A more general examination of the character of the effect of shadowing on the reflected field could be obtained by representing the terrain elevation along a radial as a random function of distance from the sensor. One such representation would be a function of the type used to characterize a Gaussian process. If the probability that a point on the terrain will be visible to a source located at infinity $S_G(\theta)$, a statistical measure of shadowing may be derived. This approach was taken in Reference 5, and the probability of shadowing as a function of elevation angle is

$$S_G(\theta) = (1 + \text{erf } v) \left(1 - \frac{\exp(-2B)}{4B}\right) \qquad (22)$$

where

$$v = \tan \theta / \sqrt{2 \left| \psi_0'' \right|}$$

$$B = [\exp(-v^2) - \sqrt{\pi v} \, \text{erfc } v]/4\sqrt{\pi} \, v$$

51

$$\psi_0 = E[h(r) \, h(r)]$$

$$\psi_0'' = \left[\frac{\partial^2}{\partial \tau^2} \, E[h(r) \, h(r + \tau)] \right]_{\tau = 0}$$

h(r) is the Gaussian process describing the terrain

contour as a function of range.

A plot of $S_G(\theta)$ is given in Fig. 25 for a Gaussian process with an auto-correlation function $\varphi(\tau) = \sigma^2 \exp(-\tau/T)$. It may be seen from Fig. 25 that as the terrain roughness increases, i.e., σ/T increases, the probability of a point being shadowed increases. Also note that at zero elevation angle, the visibility of the terrain is very low.

Another way to depict shadowing, a method that emphasizes the shadow cast by major hills, is to represent the hills as vertical obstructions with a random distribution of heights and with a Poisson rate of occurrence in range as shown in Fig. 26.

If the hills occur with mean distance ΔR and with Poisson rate of occurrence in range, the probability that there would be no hill within a distance R short of a point is

$$P[\text{no hill within distance R}] = \exp(-R/\Delta R) \quad . \tag{23}$$

If the aircraft is at an elevation angle θ, a hill with a height h casts no shadow on a point if the hill distance R to the left of the point obeys the following relation:

$$R \geq \frac{h}{\tan g \ \theta} \qquad .$$

If the hills have a height distribution $P_H(h)$, then the probability that a point will not be shadowed is

$$S_P(\theta) = \exp\left(-\frac{\overline{h}}{\Delta K * \tan \theta}\right) \qquad (25)$$

$$\overline{h} = \int P_H(h) * H \ dh \qquad .$$

Equation 25 shows that as the heights increase (i. e., $\overline{h}$ increases) or their frequency increases (i. e., ΔR decreases), there is less terrain visible.

Figure 27 gives representative plots of Equation 25. It is seen again that for aircrafts at the horizon, no terrain is visible. For a terrain with hills approximately 100 ft above their surroundings and separated by approximately 10,000 ft ($\overline{h}/\Delta R = 0.01$), most of the terrain becomes visible when the ray's elevation angle is a few degrees above the horizon as indicated in Fig. 27.

The terrain that is visible for reflection is reduced because of the obstructions in the direction of the sensor as well as in the direction of the aircraft. If most of the reflection occurs at a terrain that subtends the same angle θ toward the sensor as it does toward the aircraft, and the reflected field is linearly proportional to the visible terrain, then the shadowing reduction of reflected field would be given by

53

$$r_S(\theta) = \begin{cases} S_G^2(\theta) \\ \\ \\ S_P^2(\theta) \end{cases} \qquad (26)$$

depending on whether Equation 22 or Equation 25 is used for shadowing.

The assumption, that the terrain from which most of the field is reflected subtends an angle θ at the sensor, is not completely correct. The terrain that reflects the field subtends an angle at the sensor between ninety degrees for terrain next to the sensor, and zero degrees above horizon for terrain far away. If the reflecting terrain is uniformly dispersed along range, each terrain increment in range will have a fraction $R_i(\theta_a, \theta_S)$ visible to both the sensor and the aircraft

$$R_i( ) = S_i(\theta) * S_i(\theta_S) \qquad i = \begin{cases} G \\ P \end{cases} \qquad (27)$$

where

θ is the angle subtended by the terrain increment at the aircraft

θ_S is the angle subtended by the terrain increment at the sensor

$S_i( )$ is the shadowing function based on Gaussian or Poisson models

Shadowing introduces a scalar reduction of the field (expression 27); thus, the reflected field reduction $r_S(\theta)$ is

$$r_i(\theta) = \left| \frac{1}{\sqrt{2}} \int_{-\infty}^{\infty} S_i(\theta) S_i(\theta_S) \exp\left(j \frac{\pi}{2} * \eta^2\right) d\eta \right| \qquad i = \begin{matrix} G \\ P \end{matrix} \;.$$

$$(28\text{-}a)$$
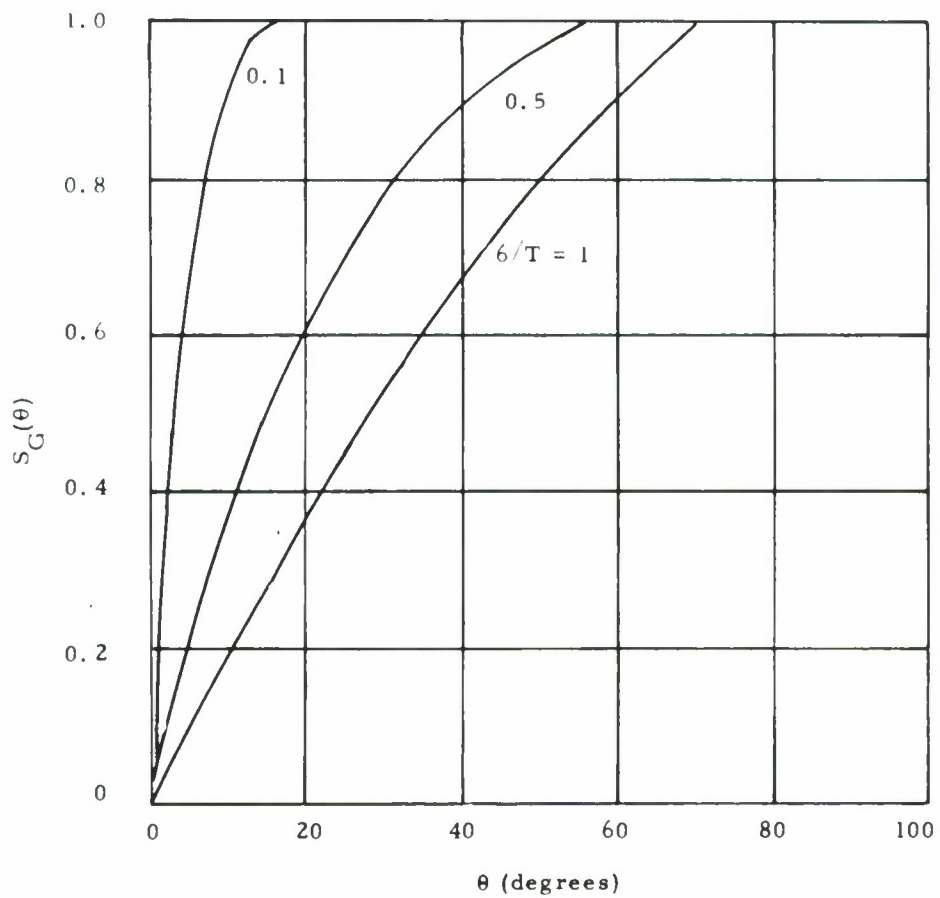
Fig. 25. Comparison of shadowing ($S_G(\theta)$) for a Guassian process with autocorrelation function $\sigma^2 e^{-\tau}/T$ as a function of elevation angle (θ).
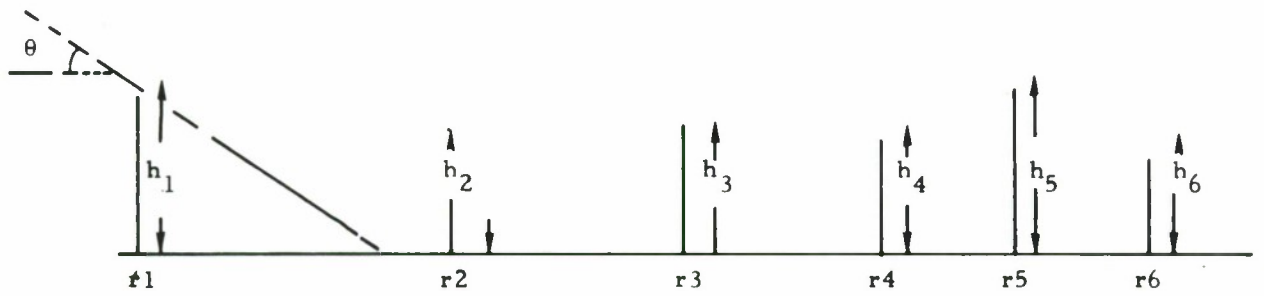
Fig. 26. Representation of hills as vertical obstruction with Poisson occurrence in range.
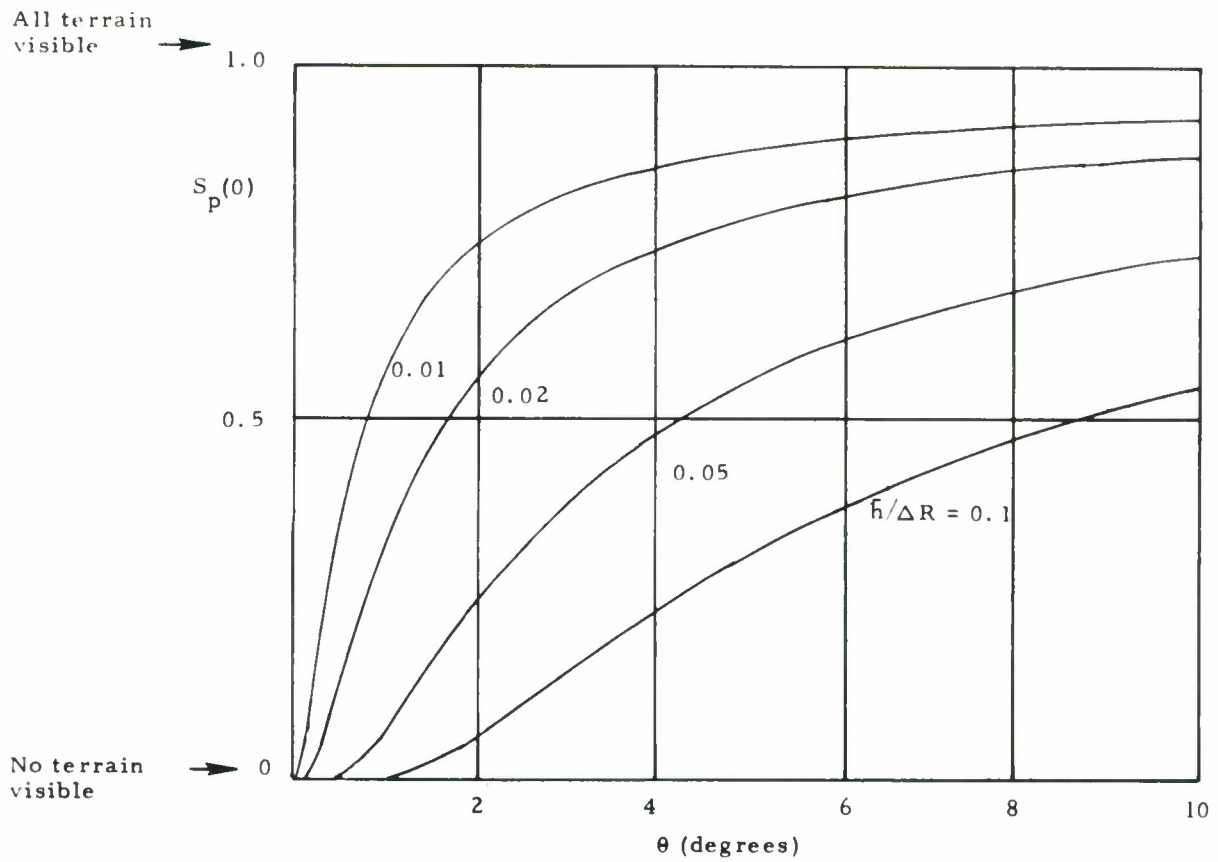
Fig. 27. Probability of hill shadows (Sp) as a function of elevation angle θ; mean hill height to hill distance $\bar{h}/\Delta R$. Poisson model is used to represent hill distribution.

The geometry of this problem is similar to that corresponding to a sensor in a limited flat earth given in Chapter III. The difference is that the integration limits in Equation 28 are over $-\infty$ to ∞ with a field reduction factor corresponding to shadowing introduced inside the integral. In Equation 28, the variable of integration has a value η corresponding to a terrain increment at a distance, d, from the sensor. The value of η is

$$\eta = \sqrt{\frac{2}{\lambda * d}} \; * (h - d * \theta) \qquad (28\text{-}b)$$

for $\quad \theta << 1$
$\quad\quad\; d >> h$

where again

h is the antenna height

θ is the aircraft elevation in radians

The sensor elevation angle θ_S above horizon with respect to the terrain increment at a distance, d, is

$$\theta_S = \tan^{-1} \frac{h}{d}$$
$$\approx \frac{h}{d} \qquad (28\text{-}c)$$

where

θ_S is assumed to be in radians.

Use of Equations 28-b and 28-c gives

$$\theta_S = \left(\sqrt{C^2 + 4 * \theta} + C\right)^2 / 4 \qquad (28-d)$$

where

$$C = \eta * \sqrt{\frac{\lambda}{2 * h}} \qquad .$$

Thus, for a given aircraft elevation angle θ, the reduction $r_i(\theta)$ in the reflected field due to shadowing is

$$r_i(\theta) = S_i(\theta) * S_{is}(\theta) \qquad (29-a)$$

where

$S_{is}(\theta)$ is the sensor effective shadow field reduction

$$S_{is}(\theta) = \frac{1}{\sqrt{2}} \left| \int_{-\alpha}^{\alpha} S_i(\theta_S) \exp\left(j \frac{\pi}{2} \eta^2\right) d\eta \right| \qquad i = \begin{cases} P \\ G \end{cases} \qquad (29-b)$$

with θ_S given by Equation 28-d, and $S_i(\theta)$ given by Equation 22 or 25 depending on the terrain shadowing model used.

From Equation 29, it follows that $S_{is}(\theta)$, the sensor effective shadow field reduction, is not necessarily equal to reflected field reduction due to aircraft shadowing given by $S_i(\theta)$.

The effect of shadowing on the reflected field is examined for the following example

$$\lambda = 1 \text{ ft}$$

h (antenna height above surrounding terrain) = 100 ft

Poisson model for hills with mean hill height to hill separation $\bar{h}/\Delta R = 0.01$.

In Fig. 28, dashed curves 1 and 2 respectively give the effective sensor shadow field reduction $S_{pS}(\theta)$ and the aircraft shadow $S_p(\theta)$. From the figure it is noticed that the former is always larger than the latter by approximately 5 percent. Examining both curves shows that shadow effect diminishes greatly at an elevation angle above a couple of degrees. In the same figure, solid curves 3 and 4 respectively give the total effect of shadowing $R_p(\theta)$ and $r_p(\theta)$ on reflected field computed by Equations 26 and 28, respectively. In the present example, neglecting the proximity of the sensor to the reflecting terrain would give a reflected field smaller by about 5% compared to the field reflected when account is taken of this effect.

The effect of decreasing the mean hill height to hill spacing from 0.01 to 0.005 is shown in Fig. 29. To a first order approximation, multiplying $\frac{\bar{h}}{\Delta R}$ by a factor D would produce the same effect on shadowing at an elevation angle $[(\theta) * D]$, that would have occurred at an elevation angle θ previously, i.e.,

$$\frac{\bar{h}}{\Delta R} \longrightarrow \frac{\bar{h}}{\Delta R} * D$$

$$r_p(\theta) \longrightarrow r_p(\theta/D) \quad .$$

60
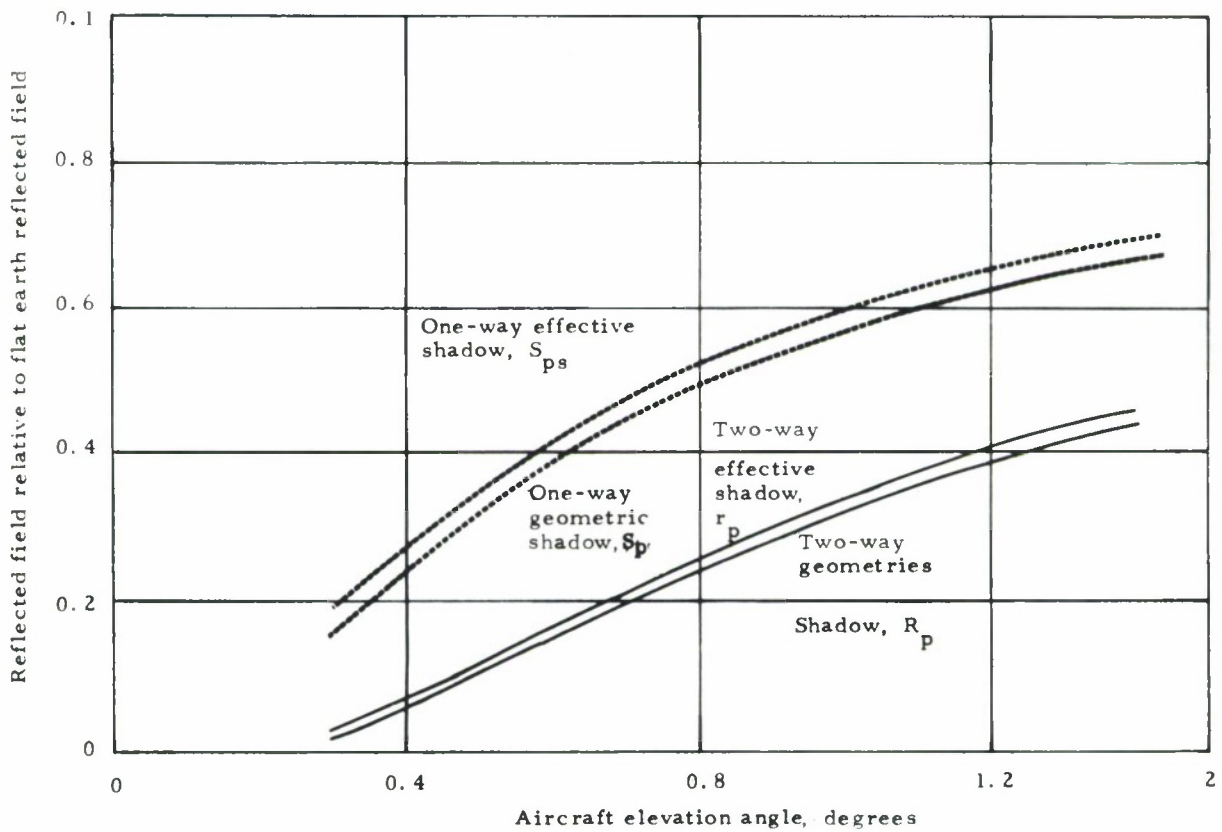
Fig. 28. Effect of shadowing on reflected field for a Poisson model of hills; mean hill height to spacing is 0.01.
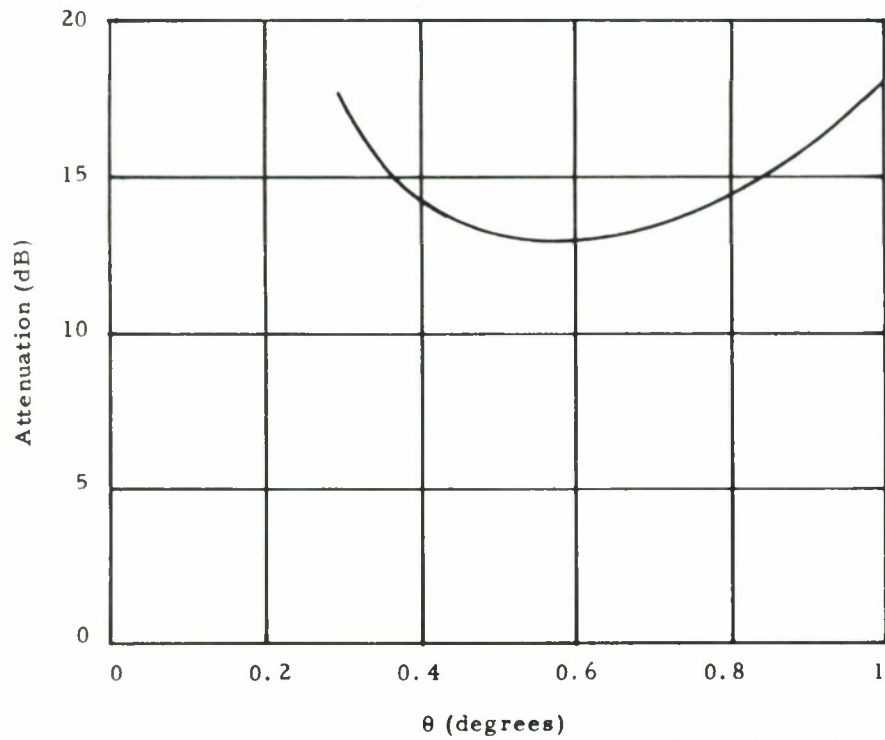
Fig. 29. The effect of mean hill height to spacing $\bar{h}/\Delta R$) on the shadow as a function of aircraft elevation.

This is illustrated in Fig. 29 and is seen from the following relation obtained from Equation 25.

$$S_p(\theta) = \exp - (\bar{h}/\triangle R/\theta)$$

$$\approx \exp - (\bar{h}/\triangle R/\theta)$$

$$\text{for } \theta < < 1 \quad .$$

Let $S_{1p}(\theta)$ be the function obtained from $S_p(\theta)$ by multiplying $\bar{h}/\triangle R$ by D. Then we have

$$S_{1p}(\theta) = \exp(-D * (\bar{h}/\triangle R)/\theta)$$

$$= \exp(-(\bar{h}/\triangle R)/(\theta/D))$$

$$= S_p(\theta/D)$$

which explains the observation made above.

Next consider the effect of local roughness on the magnitude of the reflected field. Ament [Ref. 6] gives the following formula for $rs(\theta)$, which is the reduction of the reflected field due to scattering from a randomly rough surface, compared to a flat surface

$$rs(\theta) = \exp\left(-2\left(\frac{2\pi H \sin \theta}{\lambda}\right)^2\right)$$

$$\text{for } H \frac{\sin \theta}{\lambda} < 0.1$$

63
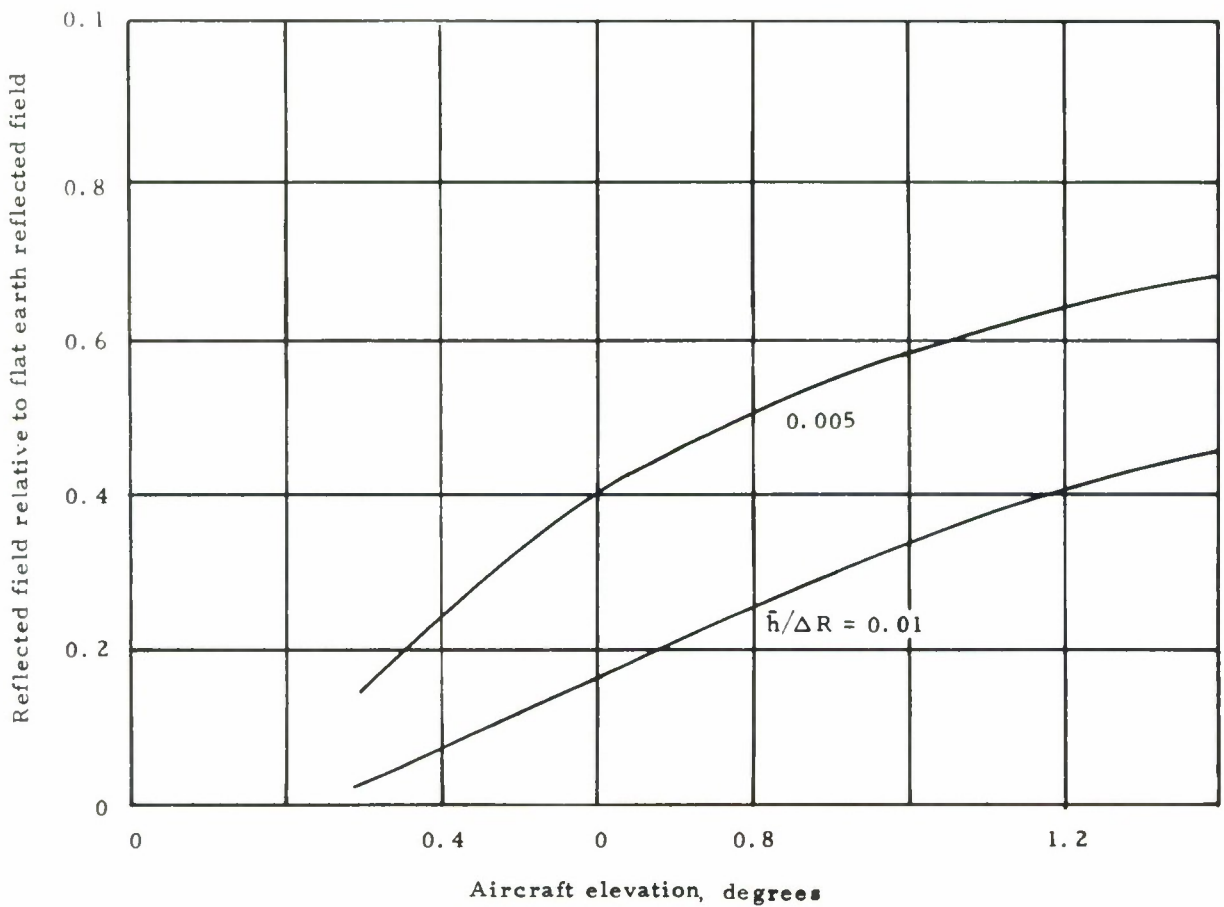
Fig. 30. Attenuation of reflected field by shadowing ($\Delta H/R = 0.005$) and scattering (RMS = 8 ft) as a function aircraft elevation θ.

where

H is the standard deviation of the surface distribution.

For purposes of illustration, the attenuation of the reflected field is given for a terrain described by the example mentioned in this chapter with $\bar{h}/\Delta R = 0.005$, and H = 8 ft. Figure 30 gives the attenuation due to shadowing and scattering. The total reflected field attenuation is between 12 dB and 17 dB for elevation angles between 0.25 degree and 1.0 degree.

APPENDIX A

ANTENNA CUTOFF EFFECT ON LIMITED
FLAT EARTH REFLECTION

The value of K, in Equation 9 of Section 3, is based on a simplifying assumption that the antenna gain is constant with respect to elevation angle. The sensitivity of K^* to antenna cutoff is examined by computing an equivalent K'(Ant, h, d, φ) defined as

$$K'(\text{Antenna, } h, d, \varphi, \lambda)$$

$$= \frac{\frac{1}{2j} \int_{\eta_1}^{\infty} F\left(\frac{h}{d} - \frac{\eta\lambda}{2 * d}\right) * \exp\left(j \frac{\pi\eta^2}{2}\right) d\eta}{F(\varphi)} \tag{A-1}$$

where

F(φ) is the field strength of the antenna at an elevation angle of φ below horizon.

K' more explicitly takes into account the nonuniform illumination of the aperture in the path of the field coming from the antenna image. K' reduces to K (defined in Equation 9), and the antenna gain, F(φ), is constant as a function of elevation angle φ. The relative accuracy of K as compared to K' was examined

---

[*]Initial discussion with J. Evans led to the work reported here.

66

by computing K and K'. This was done for antenna heights of 200 ft and a limited flat dry earth extending to 15,000 ft, and a wavelength of λ = 1 ft. The first two peaks of K and K' would occur for the above conditions within the first two degrees elevation above horizon. The antenna elevation patterns used in the study are the DABSEF antenna with a cutoff of 3.0 dB/deg at horizon and the modified ASR integral feed that has a cutoff of 1.5 dB/deg at horizon.

The results are shown in Fig. A-1 for the DABSEF antenna and in Fig. A-2 for the ASR antenna. It is seen that in both cases there is a close fit between $|K|$ and $|K'|$ for elevation angles lower than 0.8 degree. The deviation between $|K|$ and $|K'|$ becomes larger for higher elevation angles or sharper cutoff antennas. Table A-1 gives the largest and next largest values of K and K'.

TABLE A-1

EFFECT OF ANTENNA CUTOFF ON LIMITED

SURFACE MODIFICATION OF REFLECTED FIELD

| Antenna Cutoff, dB/deg	At first peak		At second peak	
	$|K|$	$|K'|$	$|K|$	$|K'|$
1.5	1.17	1.19	1.095	1.124
3	1.18	1.21	1.095	1.15
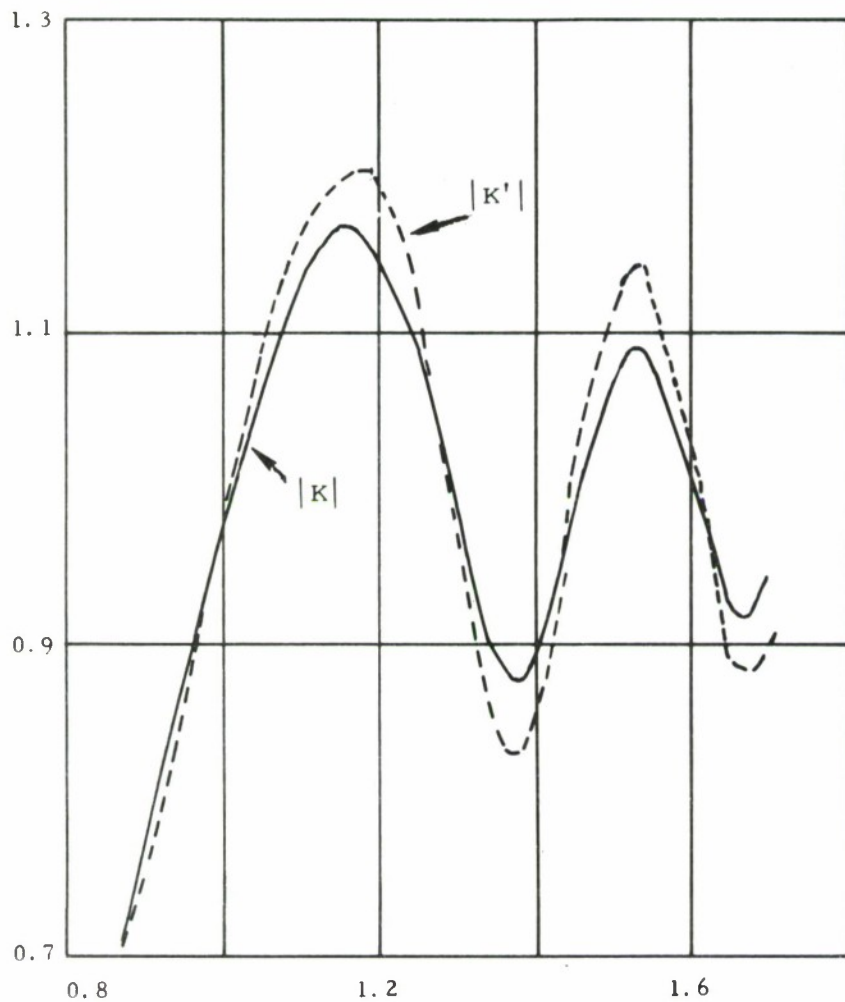
Fig. A-1. Values of $|K|$ and $|K'|$, the magnitude of the modification of reflection due to limited surface extending to 15,000 ft as a function of elevation θ. Antenna height is 200 ft; DABSEF antenna elevation pattern is used.
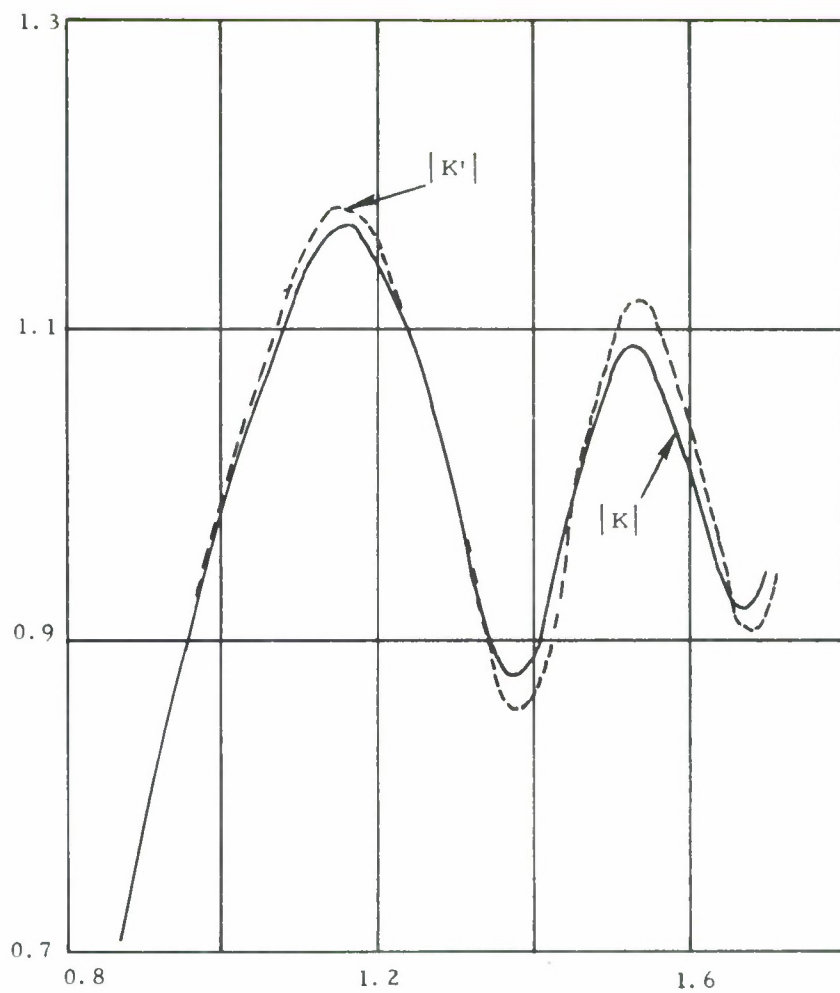
Fig. A-2. Value of $|K|$ and $|K'|$, the magnitude of the modification of reflection due to limited surface extending to 15,000 ft vs elevation (θ). Antenna height is 200 ft; modified integral feed ASR antenna is used.

A similar deviation was observed between the peak values of $|K|$ and $|K'|$ for other antenna heights and limited flat surface extents.

The sensitivity of the fades magnitude to K was also examined. This was done at the peak value of K where a relatively high accuracy of K is needed. Suppose the conditions are such that a null in the lobing pattern occurs at 0.75-degree and 1.3-degree elevation, and that the first and second peak of K occur at these angles. Table A-2 gives the magnitude of fades with respect to free space again at these angles, using both K and K' for computing the effect of limited flat earth.

TABLE A-2

FADES WITH RESPECT TO FREE SPACE GAIN

USING $|K|$ AND $|K'|$

Antenna cut-off dB/deg	FADE			
	At 0.75 deg		At 1.3 deg	
	$|K|$	$|K'|$	$|K|$	$|K'|$
1.5	15.2	16.0	8.9	9.3
3.0	8.8	7.2	4.8	4.9

It may be noticed that using K to characterize the effect of limited flat surface reflection could not introduce errors in the fades of more than 1.0 dB for the 1.5 dB/deg cutoff antenna, and not more than 2.0 dB for the 3.0 dB/deg.

Comparing the magnitude of K with K' at the first peak of each, it is seen that the value of $|K'|$ increases at the rate of 0.0133 above 1.17 for each dB/deg cutoff of the antenna. This number could be used as a correction factor for the difference between K and K' as a function of the antenna cutoff up to 3 dB/deg, a range covering existing candidates for DABS antennas.

70

APPENDIX B

DIFFRACTION LOSS OVER A ROUNDED HILLTOP

Consider a sensor situated such that a rounded hill exists in the path of its direct field, as shown in Fig. B-1. If the hill has a curvature radius of r, and is at a range R from the sensor, then the fade loss would be as shown in Fig. B-2. The parameter ρ defines a measure of curvature, and η is the parameter analogous to the one defined in Equation 2. The following equations define these two parameters explicitly:

$$\eta = \sqrt{\frac{2R}{\lambda}} * \tan \theta$$

$$\rho = 0.0826 \left(\frac{r}{\lambda}\right)^{1/3} \times \left(\frac{\lambda}{R}\right)^{1/2}$$

where

θ is the elevation angle of the aircraft above the hilltop

R is the range of the hill from the sensor

r is the radius of curvature of the hilltop.
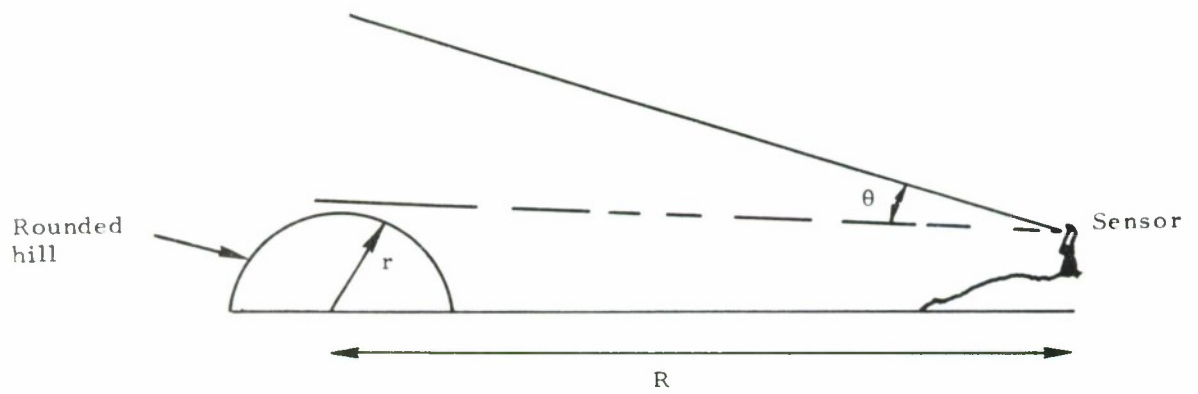
Fig. B-1. Parameters for rounded hilltop diffraction
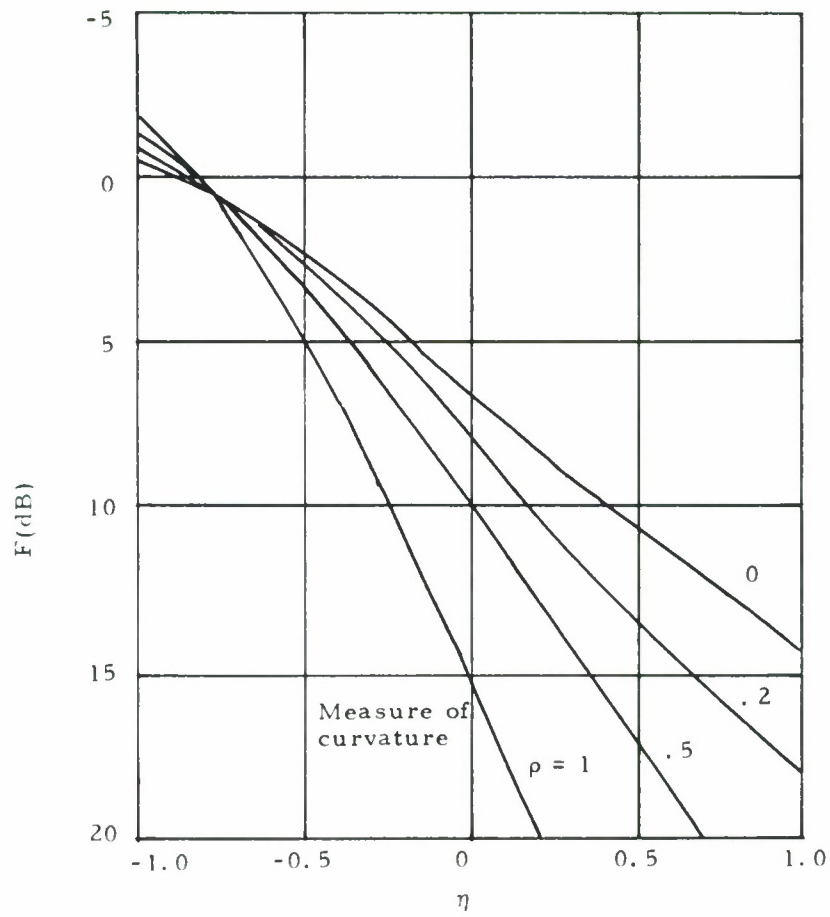
Fig. B-2. Fade (F) due to diffraction over a rounded hilltop.

73

APPENDIX C

REFRACTION IN THE ENVIRONMENT

The effects of stratification of the earth's atmosphere upon RF rays and, in turn, upon the effective speed of these rays, are discussed in this section.

A summary of the refraction variation with time and location, with better models to represent it, is reported here (taken from References 7 and 8). The effect of this variation on vertical lobing is analyzed. Also reported is the effect of refraction on DABS range error and a method to reduce the effect.

Effective Earth Radius (k * a)

For the purpose of clarity the concept of effective earth radius is explicitly defined here. In Fig. C-1, a sketch of a ray track is shown. In Fig. C-2, the corresponding effective earth model is shown.

Essentially in Fig. C-2 the radius of the earth has been increased so that point P will be at the same altitude h above the surface, as in Fig. C-1a, but the radio ray will be a straight line with the same initial elevation angle.

Description of Atmosphere

The speed of light tends to increase with altitude corresponding to a decrease in the refraction index, n, with altitude. If the refraction index is
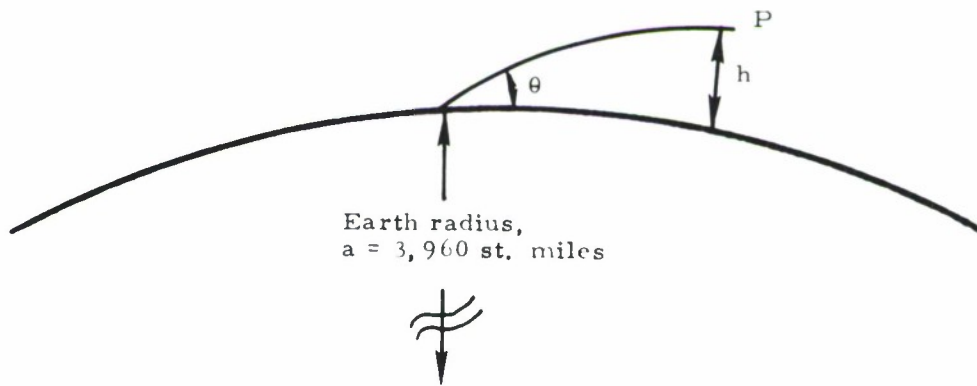
Fig. C-1.   Ray trace above normal earth radius surface.
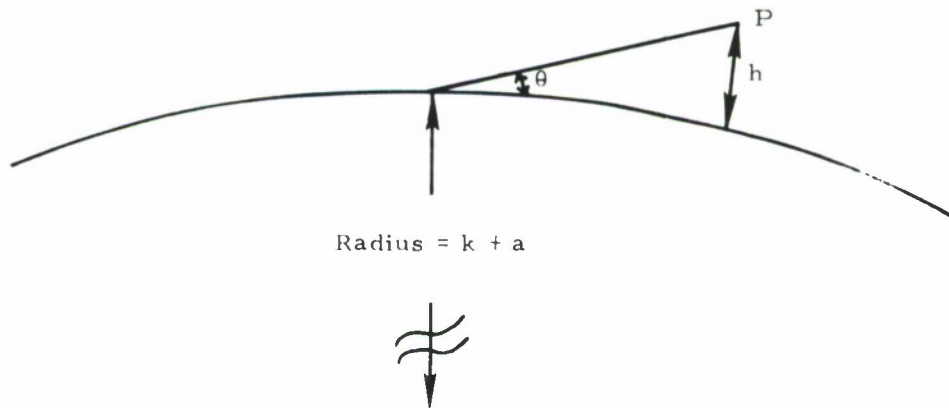
Fig. C-2.   A straightened ray trace above an equivalent earth radius k * a.

is assumed to increase at a constant rate $\dfrac{dn}{dn}$ with altitude h, then the effective earth radius is given [Ref. 8] by k * a where a is the radius of the earth.

$$k = \dfrac{1}{1 + \dfrac{a}{n}\dfrac{dn}{dh}} \quad .$$

It is usually assumed that

a = 3,960 statute miles

$\dfrac{dn}{dh}$ of the order of $-40 \times 10^{-6}/km$

n = 1.0003   .

These would then correspond to the familiar k = 4/3. Another way of representing the refraction of a medium is by N, the refractivity, defined as

$$N = (n - 1) * 10^{6} \quad .$$

Typical values of N, as given in Reference 7, are shown in Fig. C-3 as a function of altitude, and in Figs. C-4 and C-5 as functions of time and location. These values correspond to sea level altitude. It may be noticed in Figs. C-4 and C-5 that the refractive index is higher in summer than in winter.

It is also possible to use the U.S. Standard Atmosphere in a table lookup procedure to describe the propagation refraction. This method is used in the ray tracing algorithm of Reference 7.

76
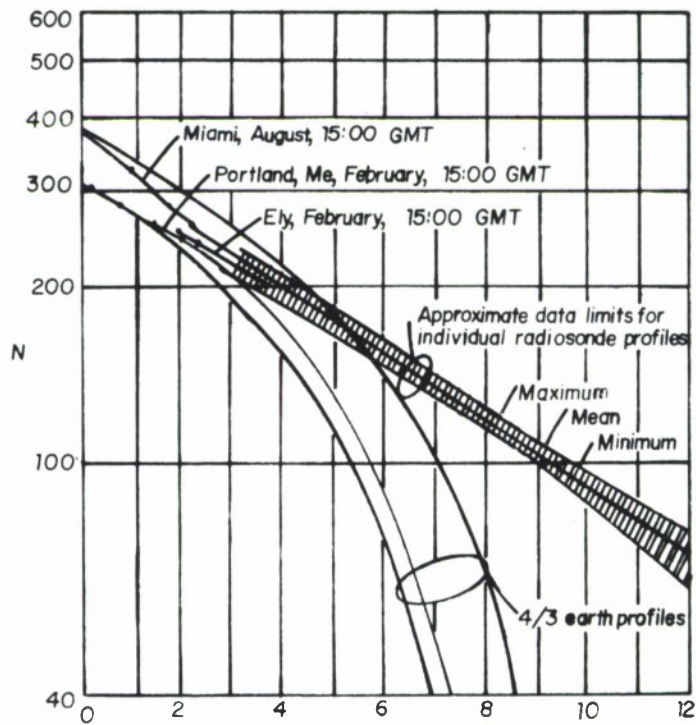
Altitude above mean sea level (kilometers).

Fig. C-3. Typical refractivity (N) vs height above earth.
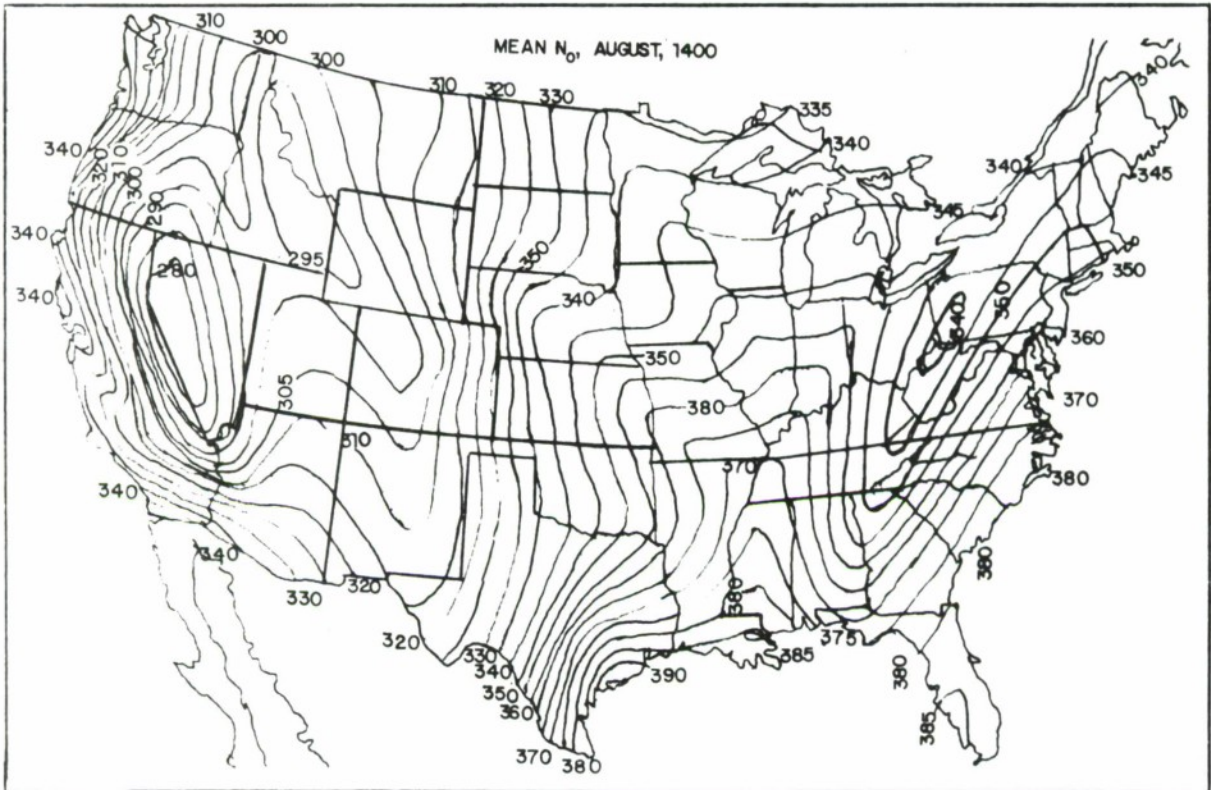
Fig. C-4. Reduced-to-sea level refractivity typical of summer days as represented by 1400 local time during August.
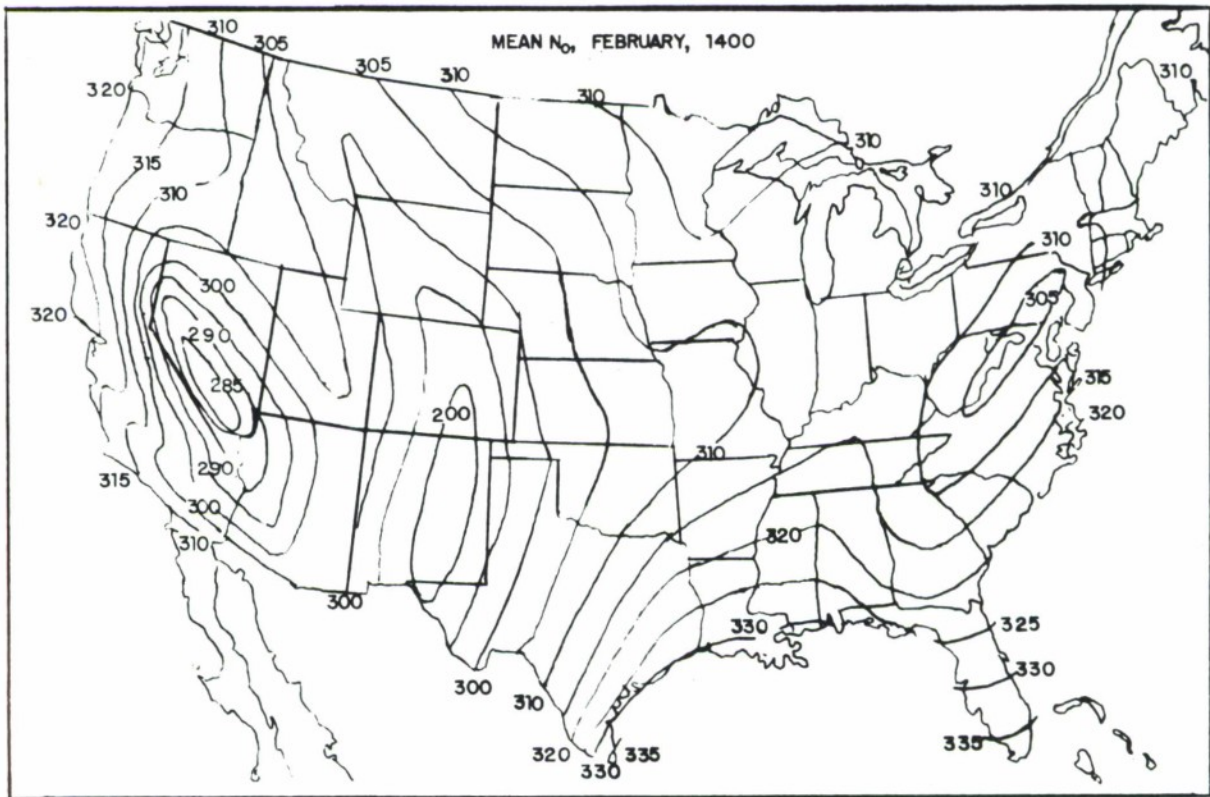
Fig. C-5. Reduced-to-sea level refractivity typical of winter days as represented by 1400 local time during February.

Spread in Effective Earth Radius

The extent to which the value of k and N_S can vary is illustrated in
Fig. C-6 (obtained from Reference 6). These plots are for a maximum altitude
of 10 km, and initial elevation angles of 0. 1 degree and 2. 0 degrees. The
scatter points are for 318 atmospheric profiles. It may be seen that the value
of k could vary from 1. 2 to 2. 2 corresponding to a range variation of 35% for
the case at hand.

The spread in the distance tends to increase with altitude and decrease
in initial elevation angles. Also, ray end points tend to be at the shorter range
in winter than in summer. Figure C-7 sketches an upper bound on the expected
spread in range as a function of initial elevation angle of the ray for a point
at 14, 000 feet in altitude. Notice that the bound is of the order of 10 nmi for
an elevation angle of 0. 5 degree.

Range Error

Refraction causes bending of RF rays. Also, because of refraction,
the rays travel at different speeds at different altitudes. Figure C-8 illustrates
this situation.

R_0 is the true range; the "measured" range R_e would be

$$R_e = \int_0^R n * dR$$

where n is the index of refraction. Thus, the range error would be

$$\Delta R_e = R_e - R_o \quad .$$

80
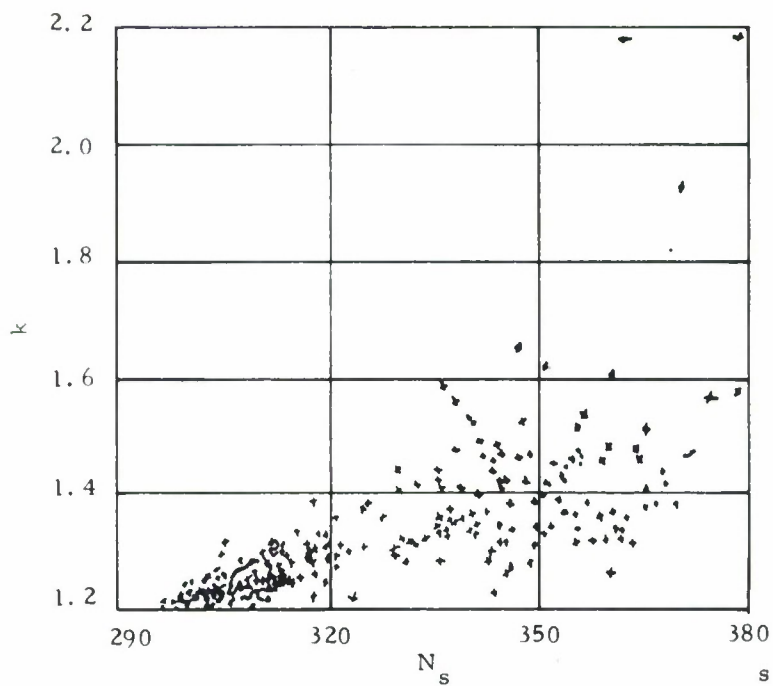
Fig. C-6. Spread of surface refractivity N_s, and k the increase of an effective radius for initial elevation angle of 2 degrees. Final altitude is 10 km.
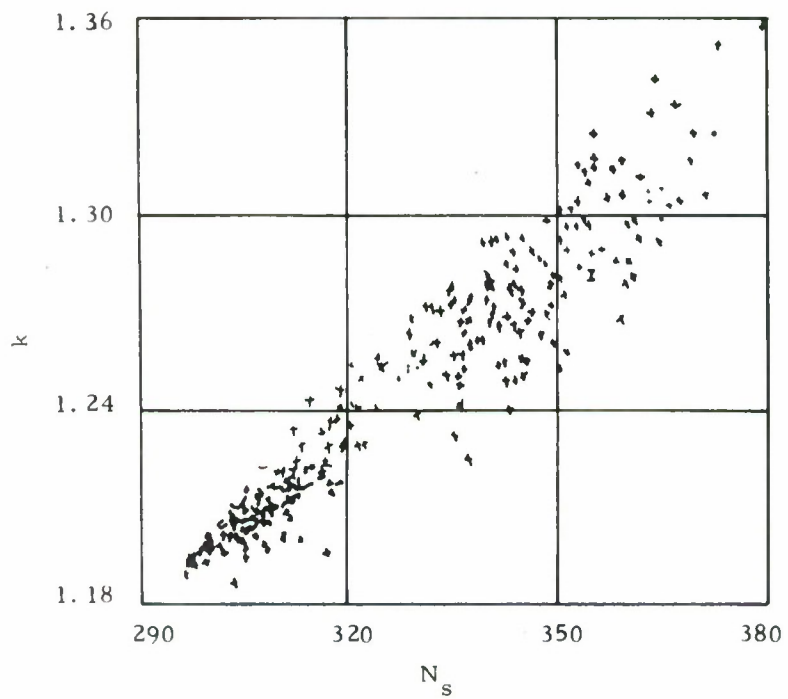
Fig. C-7. Spread of surface refractivity N_s, and k the increase of an effective earth radius for initial elevation angle of 2 degrees. Final altitude is 10 km.
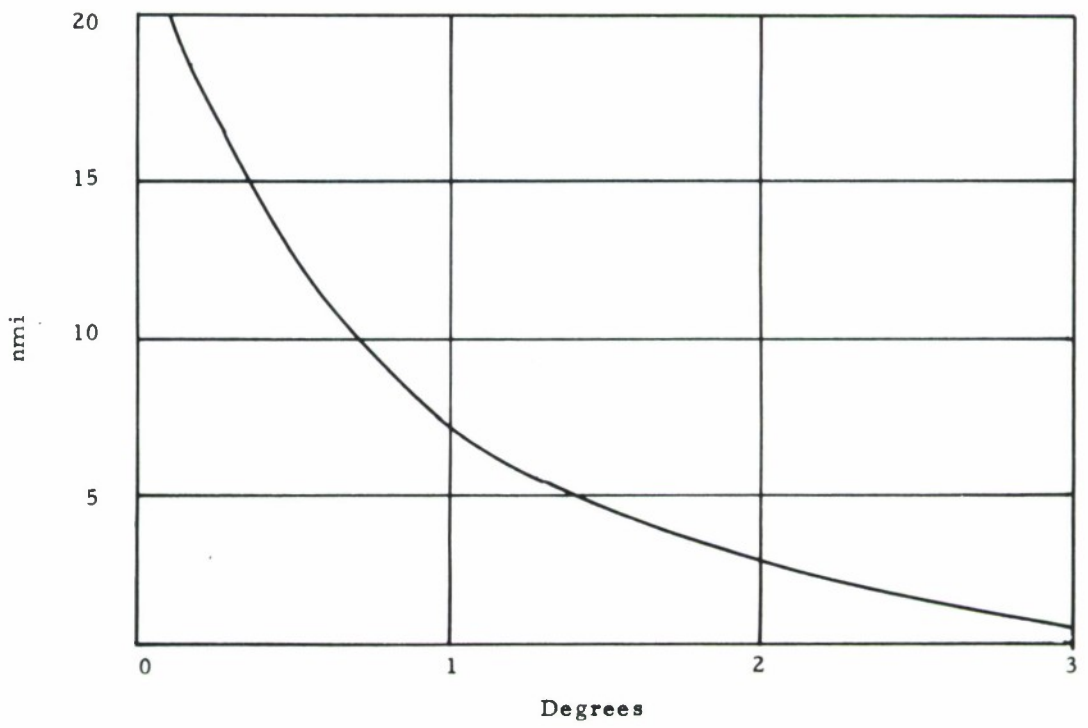
Fig. C-8. Upper bound on the expected spread in range of a ray that attains an altitude of 14,000 ft as a function of initial elevation angle of it.

Figure C-9 is based upon the use of operational software from Reference 6 to give the range error as a function of range for the mean U.S. Atmosphere (January and July). The sample points are specified by the combination of starting elevation angles and altitudes given in Table C-1. The mean error in range for this set is 1.72 ft/nmi. A formula for a best linear fit of error vs range would be

$$\Delta R_e = 1.7 * R_e \quad .$$

Using this expression would give a mean deviation of the actual error from the calculated error of less than 1/20 ft per nmi.

TABLE C-1

THE INITIAL ELEVATION ANGLES AND FINAL

ALTITUDES USED IN GENERATING DATA FOR FIG. C-9[*]

Altitude (feet)	Elevation Angle (degrees)
1700	0
2300	0.3
3300	0.6
4300	1
5300	1.4
—	2
7300	3

[*]Initial altitude is assumed to be 300 ft.

84
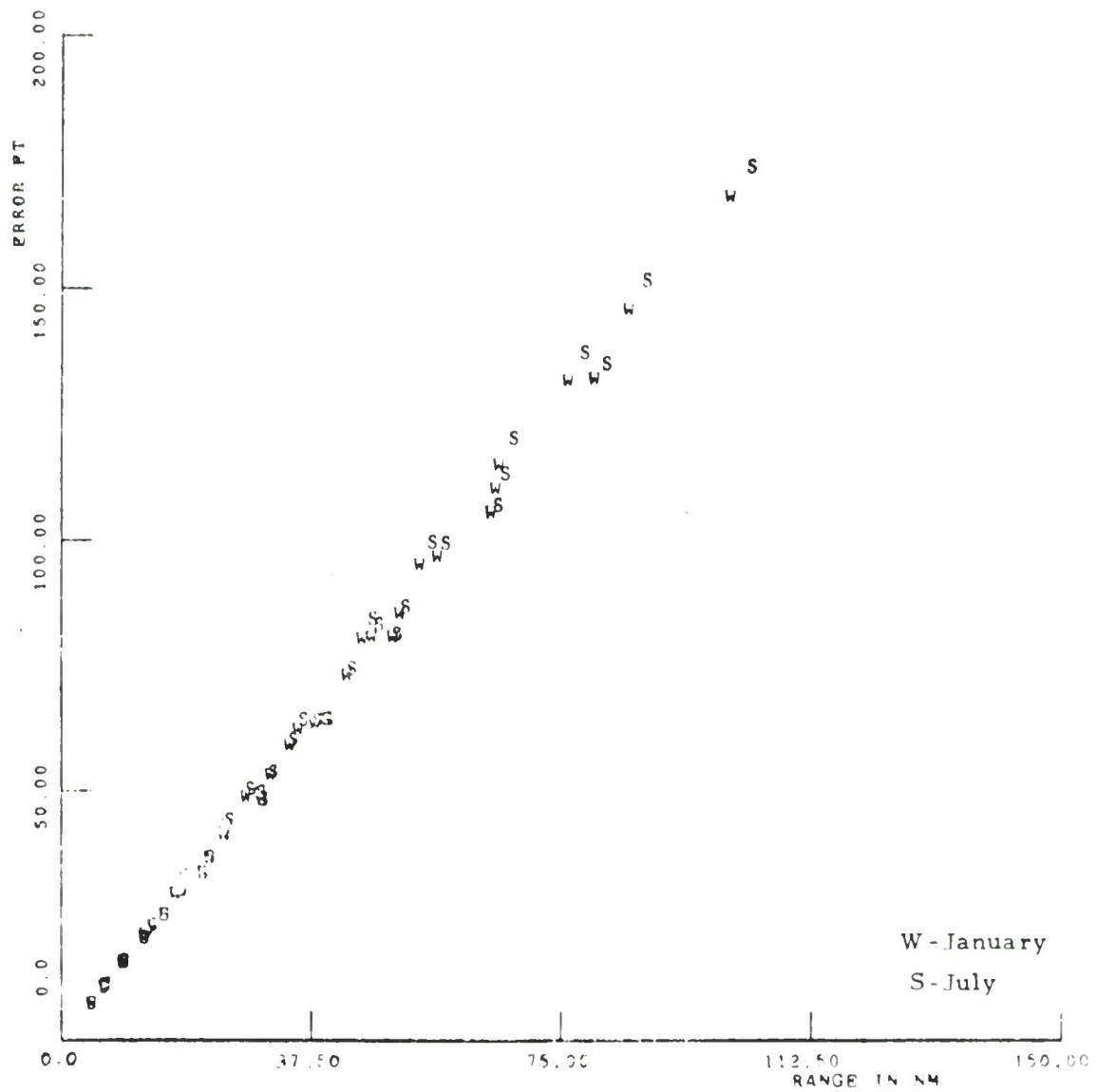
Fig. C-9. Range error vs range for January and July corresponding to standard atmosphere.

In the operation of DABS, it is possible to reduce the range error (due to refraction) by using a speed of light less than the free space speed of light, by a factor of

$$\frac{6076 - 1.72}{6076} = 0.99972 \qquad .$$

REFERENCES

[1]   J. W. Goodman, Introduction to Fourier Optics (McGraw-Hill, New York, 1968).

[2]   G. Millington et al., "Double Knife-Edge Diffraction in Field Strength Predictions," Monograph No. 507E, Proc. Inst. Elect. Eng. 109C, pp. 419-429 (September 1962).

[3]   G. Millington et al., "The Fresnel Surface Integral," Monograph No. 507E, Proc. Inst. Elect. Eng. 109C, pp. 430-437 (September 1962).

[4]   P. L. Rice et al., "Transmission Loss Predictions for Tropospheric Communication Circuits," National Bureau of Standards Technical Note No. 101, Volume 1 (Revised) (U. S. Government Printing Office, Washington, D. C., January 1967), DDC AD-687820 and AD-687821.

[5]   R. J. Wagner, "Shadowing Randomly Rough Surfaces," J. Acoust. Soc. Am. 41, pp. 138-145 (1967).

[6]   W. S. Ament, "Toward a Theory of Reflection by a Rough Surface," Proc. IRE 41, pp. 142-146 (1967).

[7]   R. K. Crane, unpublished work.

[8]   B. R. Bean and G. D. Thayer, "Models of Atmospheric Radio Refractive Index," Proc. IRE 47, pp. 740-755 (1959).